NASA
Technical
Paper
3283

January 1993

An Optimization-Based Integrated Controls-Structures Design Methodology for Flexible Space Structures

Peiman G. Maghami,
Suresh M. Joshi,
and Ernest S. Armstrong

NASA

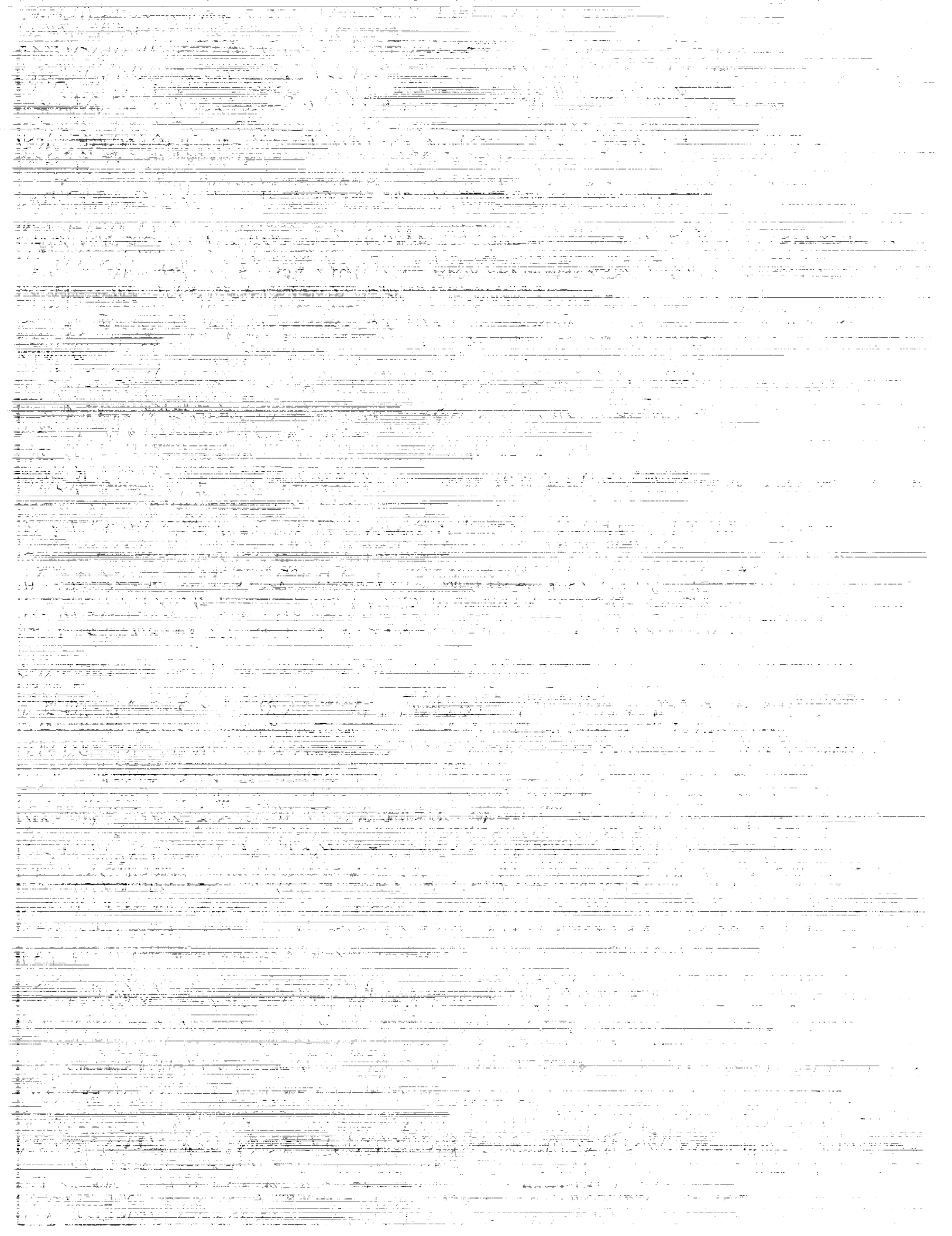

NASA Technical Paper 3283

1993

An Optimization-Based Integrated Controls-Structures Design Methodology for Flexible Space Structures

Peiman G. Maghami,
Suresh M. Joshi,
and Ernest S. Armstrong
Langley Research Center
Hampton, Virginia

National Aeronautics and Space Administration
Office of Management
Scientific and Technical Information Program

The use of trademarks or names of manufacturers in this report is for accurate reporting and does not constitute an official endorsement, either expressed or implied, of such products or manufacturers by the National Aeronautics and Space Administration.

Nomenclature

$\mathbf{A}$	open-loop state matrix
$\mathbf{A}_c$	state matrix for the dynamic dissipative compensator
$\mathbf{A}_{\mathrm{cl}}$	closed-loop state matrix
$\mathbf{A}_K$	state matrix for $K(s)$
$(\boldsymbol{A}, \boldsymbol{B}, \boldsymbol{C}, \boldsymbol{D})$	nth-order minimal realization of $T(s)$
a	actuator bandwidth
$\mathbf{B}$	control influence matrix (in state-space representation)
$\mathbf{B}_c$	input influence matrix for the dynamic dissipative compensator
$\mathbf{B}_K$	input influence matrix for $K(s)$
$\mathbf{C}_K$	output influence matrix for $K(s)$
$\mathbf{C}_p$	position measurement influence matrix (in state-space representation)
$\mathbf{C}_r$	rate measurement influence matrix (in state-space representation)
$\mathbf{C}_{\mathrm{per}}$	influence matrix for the performance output
$\mathbf{D}$	open-loop damping matrix
$\boldsymbol{D}_K$	feed-through matrix for $K(s)$
$\mathbf{D}_{\mathrm{r}}$	open-loop damping matrix in modal coordinate
d_i	outer diameter of tubes associated with structural design variable i
$d_{\max}$	maximum allowable outer diameter of tube
$d_{\min}$	minimum allowable outer diameter of tube
$E(\ )$	expected value of ( )
$\mathbf{e}$	pointing error vector
$e_{\max}$	pointing error tolerance
$\mathbf{G}$	gain matrix for the dynamic dissipative compensator
$\mathbf{G}_p$	position gain matrix
$\mathbf{G}_r$	rate gain matrix
$\boldsymbol{G}(\ )$	transfer function from μ to $\mathbf{y}_p$
$\boldsymbol{G}'(\ )$	transfer function from μ to $\mathbf{y}_r$
$g_a(\ )$	actuator dynamics transfer function
$\mathbf{H}$	influence matrix for $\mathbf{w}$
$\mathbf{I}_{\mathrm{r}\times\mathrm{r}}$	r $\times$ r identity matrix
$\mathbf{J}$	inertia matrix
$\mathbf{J}_{\mathrm{r}}$	inertia matrix in modal coordinate
J	objective function
j	complex number identity
$\mathbf{K}$	stiffness matrix
$\mathbf{K}_{\mathrm{r}}$	stiffness matrix in modal coordinate

$\boldsymbol{K}(s)$	compensator (controller) transfer function
$\boldsymbol{K}'$	alternate realization of $\boldsymbol{K}(s)$
k	actuator parameter
$\mathbf{L}$	Cholesky factor matrix
$\mathbf{L}_K$	Cholesky factor of the weighting matrix $\mathbf{Q}$
$\mathbf{L}_p$	Cholesky factor matrix of the position gain matrix
$\mathbf{L}_r$	Cholesky factor matrix of the rate gain matrix
l	number of position and rate measurements
M_{act}	actuator mass
M_{max}	upper bound value on mass
M_{str}	structural mass
M_{tot}	total mass
m	number of input vectors
m	number of three-axis sensors
n	order of plant
n_K	order of $\mathbf{L}_K$
$\mathbf{P}$	solution of the Kalman-Yacubovich equation
$\mathbf{P_e}$	steady-state covariance matrix of the pointing error vector
$\mathbf{P_z}$	steady-state covariance matrix of the closed-loop state vector
$\mathrm{P_c}$	controlled performance
P_{max}	upper bound value on the steady-state average control power
$\mathbf{Q}$	weighting matrix
$\mathbf{q}$	amplitude vector
$\mathbf{q_r}$	modal amplitude vector
Re( )	real part of ( )
r	number of modes in the control design model
$\mathbf{r}$	reference signal vector
$\mathbf{S}_p$	influence matrix for $\mathbf{v}_p$
$\mathbf{S}_r$	influence matrix for $\mathbf{v}_r$
s	Laplace parameter
$\boldsymbol{T}$( )	rational matrix-valued function
t	time
Tr( )	trace of ( )
$\mathbf{u}$	control input vector
$\mathbf{v}_p$	disturbance vector at the position/attitude output
$\mathbf{v}_r$	disturbance vector at the rate output
$\mathbf{W}_p$	noise intensity matrix for $\mathbf{v}_p$

$\mathbf{W}_r$	noise intensity matrix for $\mathbf{v}_r$
$\mathbf{w}$	disturbance vector at the input
$\mathbf{x}$	displacement vector
$\mathbf{x}_c$	state vector for the dynamic dissipative compensator
$\mathbf{x}_K$	state vector for $K(s)$
$\mathbf{y}_{\text{acc}}$	acceleration measurement vector
$\mathbf{y}_K$	output vector for $K(s)$
$\mathbf{y}_p$	position measurement vector
$\mathbf{y}_{\text{per}}$	performance output vector
$\mathbf{y}_r$	rate measurement vector
$\mathbf{z}$	state vector
$0_{\text{r}\times\text{r}}$	r × r null matrix
α	constant that relates the control effort to the actuator mass
β	trade-off parameter
ζ_i	damping ratio of the ith open-loop mode
$\mathbf{\Gamma}$	control influence matrix in modal coordinate
λ_i	ith eigenvalue of the closed-loop state matrix
ρ	damping ratio
$\mathbf{\Phi}_{\text{r}}$	retained open-loop eigenvector matrix
$\psi(\ )$	single-valued function
ω_i	frequency of the ith open-loop mode
$(\ )^o$	initial value of $(\ )$
$\|\ \|_\infty$	infinity norm of $\|\ \|$

Abbreviations:

ADS	Automated Design Synthesis
a.s.	asymptotically stable
CMG	control moment gyro
CSI	controls-structures interaction
EPS	Earth Pointing System
LaRC	NASA Langley Research Center
LFSS	large flexible space structure
LQG	Linear-Quadratic-Gaussian
MBC	model-based controllers
PR	positive real
rms	root mean square
SPR	Strictly Positive Real

Dots over symbol indicate derivative with respect to time; tilde over symbol indicates second-order representation; superscript ^{T} indicates a transposed matrix; and superscript * indicates complex conjugate.

Abstract

An approach for an optimization-based integrated controls-structures design is presented for a class of flexible spacecraft that require fine attitude pointing and vibration suppression. The integrated design problem is posed in the form of simultaneous optimization of both structural and control design variables. The approach is demonstrated by application to the integrated design of a generic space platform and to a model of a ground-based flexible structure. The numerical results obtained indicate that the integrated design approach can yield spacecraft designs that have substantially superior performance over a conventional design wherein the structural and control designs are performed sequentially. For example, a 40-percent reduction in the pointing error is observed along with a slight reduction in mass, or an almost twofold increase in the controlled performance is indicated with more than a 5-percent reduction in the overall mass of the spacecraft (a reduction of hundreds of kilograms).

Introduction

Current spacecraft design customarily involves an iterative sequence of designs performed separately within the structural and control disciplines. Structural design is performed first and is based on loading considerations such as would occur during launch, reboost, or component operational maneuvers. Sizes and masses of mission-related components are estimated and a structure that maintains the desired component relationships during operations is designed. A controller is next designed for the fixed structure to orient, guide, and/or move the spacecraft to obtain the required performance. The control design must also provide satisfactory closed-loop stability and robustness properties. If the nominal structure does not admit an adequate control design, it is returned to the structural discipline for modification. After modification, the structure is returned to the control discipline for redesign. This iterative process continues until a satisfactory compromise is found between the mission and control requirements. This separate-discipline approach has been successfully used in the past and works well in cases where a relatively high-stiffness structure is attainable and where nonstructural components are concentrated masses and inertias, or where performance requirements are not stringent. However, future space structures and performance requirements do not fit this category.

A number of future space missions will use large flexible structures in low-Earth and geostationary orbits. Possible structures include space science platforms, space processing facilities, and Earth observation systems. Such structures typically require large distributed-mass components such as booms, solar arrays, and antennas whose dimensions range from a few meters to possibly hundreds of meters. To minimize the costs of construction, launching, and operations, it is necessary to make the structure as light as possible. However, the combination of large size and low structural mass leads to increased flexibility and makes more difficult the control of the structure and its components to a specified precision in attitude and shape.

The combination of flexibility and low mass creates a special dynamical interaction problem that is characteristic of large flexible space structures. In the design of controllers for physical systems, some trade-off almost always has to be performed between design-model accuracy and mathematical complexity. The more accurate analysis models often require computational time that is too excessive to qualify them as design models for control purposes. Also, many of the most widely-used multivariable controller design techniques work best for moderate-order, linear, time-invariant design models. Typically, in practice, high-order nonlinear models are linearized about some operating condition and have their model order reduced to produce design models that conform to computational limitations or compensator implementation constraints. These practicalities introduce modeling errors in the form of unmodeled dynamics that must be accounted for in the controller design process. Space structure controller design models are generally found through some order-reduction procedure applied to a high-order analysis model obtained from finite element techniques. The order-reduction process essentially deletes a portion of the finite element model to produce a lower-order controller design model. Although

no longer contained in the design model, the unmodeled dynamics, represented by the deleted portion, still appear in the measurement vector and therefore can be affected by model-based control inputs. Care must be taken in the design of controllers for lightly damped systems that the control inputs do not *spillover* into the unmodeled dynamics with disastrous destabilizing effects (ref. 1).

Controls-structures interaction (CSI) in the form of destabilizing spillover has been verified in simple Earth-based laboratory experiments as well as in the design, analysis, ground development and test, and/or flight operation of space systems in industry (ref. 2). The current approach to solving CSI problems is to design the spacecraft to avoid undesired dynamical interaction. This approach generally requires either stiffening the structure or slowing down the control system response. Stiffening the structure simplifies the control design problem in that the predominant dynamics tend toward rigid body but is costly in terms of mass as well as launch packaging and weight, leading to increased fuel consumption. Slowing down the control response produces control inputs that have less of a chance of producing destabilizing effects but is costly in terms of reduced performance capability. Neither approach is completely satisfactory. What is needed is a new design approach that is capable of avoiding the damaging aspects of CSI while identifying and taking advantage of any beneficial aspects.

The development and experimental validation of such an approach is a primary purpose of NASA's CSI program (ref. 3). Fundamentally, the CSI program recognizes the high degree of coupling that exists between the control and structural disciplines when dealing with flexible structures. For example, controllers designed to be robust to unmodeled dynamics may need very low gain (and therefore, produce low performance) (ref. 4). In order to maintain high performance, it would then be necessary to redesign the structure to increase the frequencies of the higher modes likely to be affected by spillover. If the thickness of a structural member is changed, the dynamics will change, which would then change the control law and the required actuator sizes (and masses). These changes would, in turn, again change the structural model. One of the goals of the CSI program is to integrate the structures and controls design disciplines. Rather than design control and structural aspects of space structures separately in the sequential manner described earlier, approaches are being developed for a unified controls-structures modeling, analysis-and-design method that would allow a complete iteration on all critical (control and structure) design variables in a single integrated computational framework.

This paper considers missions that include flexible spacecraft with no articulated appendages and require fine attitude pointing and vibration suppression (e.g., large space antennas). Missions that involve flexible spacecraft with articulated multiple payloads, missions requiring large-angle slewing of spacecraft without articulated appendages, and missions that include general nonlinear motion of a flexible spacecraft with articulated appendages and robot arms are not considered. Two controller strategies are considered, namely, the static and dynamic dissipative controllers, which are well known for their stability robustness in the presence of unmodeled dynamics and parametric uncertainties (refs. 4 and 5). The approach selected for the development of integrated controls-structures design methodology is an optimization-based procedure employing mathematical programming techniques. The optimization approach allows freedom and variety in selecting the potentially large number of design variables. The optimization approach is also the one commonly used in the field of structural design. In fact, many papers describing optimization-based integrated design have appeared in the literature during the last 12 years. An excellent literature survey can be found in reference 6. However, only recently have applications gone beyond analytical studies with fictitious models, relatively simple laboratory apparatus, or unrealistic control designs. Some of the recent efforts include the works by Balakrishnan using infinite-dimensional models (ref. 7); by Bossi, Hunziker, and Kraft using Q-parameterization theory along with shape optimization (ref. 8); the studies by Maghami et al. on the integrated design of large structures (with thousands of degrees of freedom) using dissipative compensators (refs. 9–11); and a paper by Woodard et al. on integrated optimization with varying actuator mass (ref. 12). One of the unique features of the CSI program is that integrated designs will be fabricated and the methodology validated in the laboratory. This feature places the constraint of realism on the design process, which is not normally found elsewhere.

The purpose of this paper is to describe a portion of the integrated design methodology and results from the CSI program. This work differs from past studies in several ways. The design treats large realistic applications: a derivative of a geostationary platform designed in support of Earth observation sciences (ref. 13) and the initial phase of an evolutionary laboratory structure in the CSI program (ref. 14). A design similar to the integrated design reported

herein and that uses the CSI model is actually being constructed at the Langley Research Center (LaRC) for the purpose of validating the integrated design methodology. Also, we recognize that the effect of the control system on the structural mass and constraints can be significant when the magnitude of the control effort determines the mass of the control system and its power supply (ref. 15). This realistic effect is accounted for by the inclusion of a mathematical expression that couples the actuator masses and the controller gains. Finally, the controller formulation uses recently developed theory for dissipative controllers not previously employed in applications of this size.

We begin with a description of the mathematical model of the structure and controller design methods. Next, we offer an overview of the optimization-based integrated design procedure employed in this paper. Afterwards, descriptions of the structure, design variables and constraints, and integrated design problem statements are given for each of the applications. Finally, results from the integrated design process are discussed. An appendix giving the fundamentals of the dissipative controller theory is provided.

Mathematical Model of the Plant

The linear, time-invariant, mathematical model of a flexible space structure is given by

$$\mathbf{J}\ddot{\mathbf{x}} + \mathbf{D}\dot{\mathbf{x}} + \mathbf{K}\mathbf{x} = \widetilde{\mathbf{B}}\mathbf{u} \tag{1}$$

$$\left.\begin{aligned} \mathbf{y}_p &= \widetilde{\mathbf{C}}_p\mathbf{x} \\ \mathbf{y}_r &= \widetilde{\mathbf{C}}_r\dot{\mathbf{x}} \end{aligned}\right\} \tag{2}$$

where $\mathbf{x}$ is an $n \times 1$ displacement vector, $\mathbf{J}$ is the positive-definite inertia matrix, $\mathbf{D}$ is the open-loop damping matrix, $\mathbf{K}$ is the nonnegative-definite stiffness matrix, $\widetilde{\mathbf{B}}$ is an $n \times m$ control influence matrix, $\mathbf{u}$ is an $m \times 1$ control input vector, $\mathbf{y}_p$ and $\mathbf{y}_r$ are, respectively, $l \times 1$ position and rate measurements, and $\widetilde{\mathbf{C}}_p$ and $\widetilde{\mathbf{C}}_r$ are the corresponding output influence matrices. The second-order representation of the structure given in equation (1) is obtained through finite element modeling. The order of a large flexible space structure (LFSS) can be quite large. For design and analysis purposes, the order of the system is reduced to a design size. This reduction is accomplished by using a modal truncation approach wherein every mode in the controller bandwidth is retained and the remaining modes are truncated. The system equations in modal coordinates for the retained modes are written as

$$\mathbf{J}_\mathrm{r}\ddot{\mathbf{q}}_\mathrm{r} + \mathbf{D}_\mathrm{r}\dot{\mathbf{q}}_\mathrm{r} + \mathbf{K}_\mathrm{r}\mathbf{q}_\mathrm{r} = \mathbf{\Phi}_\mathrm{r}^T\widetilde{\mathbf{B}}\mathbf{u} \equiv \mathbf{\Gamma}^T\mathbf{u} \tag{3}$$

where $\mathbf{q}_\mathrm{r}$ is an $\mathrm{r} \times 1$ vector of modal amplitudes; $\mathbf{J}_\mathrm{r}$, $\mathbf{D}_\mathrm{r}$, $\mathbf{K}_\mathrm{r}$ are, respectively, the generalized inertia, damping, and stiffness matrices; and $\mathbf{\Phi}_\mathrm{r}$ is an $\mathrm{r} \times n$ matrix whose columns are the r open-loop eigenvectors associated with the included modes. If the mode shapes are normalized with respect to the inertia matrix, and modal damping is assumed, then $\mathbf{J}_\mathrm{r} = \mathbf{I}_{\mathrm{r}\times\mathrm{r}}$, $\mathbf{D}_\mathrm{r} = \mathrm{Diag}\,(2\zeta_1\omega_1, 2\zeta_2\omega_2, \ldots, 2\zeta_\mathrm{r}\omega_\mathrm{r})$, and $\mathbf{K}_\mathrm{r} = \mathrm{Diag}\,(\omega_1^2, \omega_2^2, \ldots, \omega_\mathrm{r}^2\}$, where ω_i and ζ_i $(i = 1, 2, \ldots, \mathrm{r})$ are the open-loop frequencies and damping ratios, respectively. Here, the sensors are collocated and compatible with the actuators, whereby

$$\left.\begin{aligned} \mathbf{y}_p &= \mathbf{\Gamma}\mathbf{q}_\mathrm{r} \\ \mathbf{y}_r &= \mathbf{\Gamma}\dot{\mathbf{q}}_\mathrm{r} \end{aligned}\right\} \tag{4}$$

Note that the collocation of the sensors and actuators is necessary for the implementation of the dissipative controllers. (See the appendix.) This collocation guarantees the system to be minimum phase (i.e., all transmission zeros are in the left-half plane) and will enhance the stability robustness of the overall system.

In defining the state vector $\mathbf{z}$,

$$\mathbf{z} = \begin{pmatrix} \mathbf{q}_\mathrm{r} & \dot{\mathbf{q}}_\mathrm{r} \end{pmatrix}^T \tag{5}$$

the dynamics of the system, assuming no appreciable sensor and/or actuator dynamics, can be written in a first-order form

$$\dot{\mathbf{z}} = \mathbf{A}\mathbf{z} + \mathbf{B}\mathbf{u} \tag{6}$$

where

$$\mathbf{A} = \begin{bmatrix} 0_{\mathrm{r}\times\mathrm{r}} & \mathbf{I}_{\mathrm{r}\times\mathrm{r}} \\ -\mathbf{K}_\mathrm{r} & -\mathbf{D}_\mathrm{r} \end{bmatrix}$$

$$\mathbf{B} = \begin{bmatrix} 0 \\ \mathbf{\Gamma}^T \end{bmatrix}$$

and

$$\mathbf{y}_p = [\mathbf{\Gamma} \quad 0]\,z \equiv \mathbf{C}_p\mathbf{z}$$

$$\mathbf{y}_r = [0 \quad \mathbf{\Gamma}]\,\mathbf{z} \equiv \mathbf{C}_r\mathbf{z}$$

The general configuration of the controlled structure is illustrated in the block diagram shown in figure 1. In this figure, $\mathbf{w}$, $\mathbf{v}_p$, and $\mathbf{v}_r$ represent disturbances at the input, position output, and the rate output, respectively; $\mathbf{r}$ denotes the reference signal vector; and $\mathbf{y}_\mathrm{per}$ refers to those outputs that are used for performance evaluations and not in the feedback loop. In this configuration, the system equations are written as

$$\dot{\mathbf{z}} = \mathbf{A}\mathbf{z} + \mathbf{B}\mathbf{u} + \mathbf{H}\mathbf{w} \tag{7}$$

$$\left.\begin{aligned} \mathbf{y}_p &= \mathbf{C}_p\mathbf{z} + \mathbf{S}_p\mathbf{v}_p \\ \mathbf{y}_r &= \mathbf{C}_r\mathbf{z} + \mathbf{S}_r\mathbf{v}_r \\ \mathbf{y}_{\text{per}} &= \mathbf{C}_{\text{per}}\mathbf{z} \end{aligned}\right\} \tag{8}$$

where $\mathbf{H}$, $\mathbf{S}_p$, and $\mathbf{S}_r$ are influence matrices for the disturbances $\mathbf{w}$, $\mathbf{v}_p$, and $\mathbf{v}_r$, respectively, and $\mathbf{C}_{\text{per}}$ is the output influence matrix associated with $\mathbf{y}_{\text{per}}$. It is assumed that $\mathbf{w}$, $\mathbf{v}_p$, and $\mathbf{v}_r$ are uncorrelated, zero-mean stationary white-noise processes with unit intensities.

Controller Design Methods

Control system design for LFSS's is a challenging problem because of their special dynamic characteristics, which include the following—a large number of structural modes within the controller bandwidth; low, closely spaced structural mode frequencies; very small inherent damping; and lack of accurate knowledge of the parameters. To implement the controller, it must be of a reasonably low order and must also satisfy the performance specifications (i.e., root mean square (rms) pointing error and closed-loop bandwidth). It must also have robustness to *nonparametric* uncertainties (i.e., unmodeled structural modes), and to *parametric* uncertainties (i.e., errors in the knowledge of the design model). Two major categories of controller design methods for LFSS are model-based controllers (MBC's) and dissipative controllers. An MBC generally consists of a state estimator (a Kalman-Bucy filter or an observer) followed by a linear-quadratic regulator. The state estimator uses the knowledge of the design model (consisting of the rotational rigid-body modes and a few elastic modes) in its prediction part. Using multivariable frequency-domain design methods, such controllers can be made robust to unmodeled structural dynamics; that is, the spillover effect can be overcome (ref. 4). However, such controllers generally tend to be very sensitive to uncertainties in the design model—in particular, to uncertainty in the structural mode frequencies (refs. 4 and 5). An analytical explanation of this instability mechanism may be found in reference 5. Achieving robustness to real parametric uncertainties is, as yet, an unsolved problem, although considerable research activity is in progress in that area.

Static Dissipative Controller

In view of the sensitivity problem of MBC's, dissipative controllers, which use collocated and compatible actuators and sensors, offer an attractive alternative. Details of dissipative controller theory may be found in the appendix. Dissipative controllers use special passivity-type input/output properties of the plant and offer robust stability in the presence of both nonparametric and parametric uncertainties (refs. 4 and 5). The simplest controller of this type is the constant-gain dissipative controller. Using collocated torque actuators and attitude and rate sensors, the constant-gain dissipative control law is given by:

$$\mathbf{u} = -\mathbf{G}_p\mathbf{y}_p - \mathbf{G}_r\mathbf{y}_r \tag{9}$$

where $\mathbf{y}_p$ and $\mathbf{y}_r$ are the measured ($3\overline{m} \times 1$, where $\overline{m}$ is the number of three-axis sensors) attitude and rate; $\mathbf{G}_p$ and $\mathbf{G}_r$ are $3\overline{m} \times 3\overline{m}$ symmetric, positive-definite gain matrices. This control law has been proven to give guaranteed closed-loop stability despite unmodeled elastic modes, parameter errors, certain types of actuator and sensor nonlinearities (such as saturation and dead zone; see the appendix for details), and first-order actuator dynamics (ref. 4). Robust stability is generally not guaranteed if the actuator dynamics are second or higher order, or in the presence of digitization, time delays, and control hysteresis. However, if acceleration feedback is permissible, it is possible to obtain guaranteed stability for second-order actuator dynamics (refs. 5 and 16). For practical space implementation, rate measurements may be obtained from rate gyros and attitude measurements may be provided by star sensors. However, if linear velocity is required (e.g., in the case of ground-based experiments) velocity signals can be obtained by integrating accelerometer signals with the aid of washout filters to asymptotically remove the accelerometer bias. The inclusion of washout filters would, however, hinder the dissipativity of this control design. Finally, the drawback of this controller is that the achievable performance is inherently limited because of its simple mathematical structure.

Dynamic Dissipative Controller

To obtain higher performance and still retain the highly desirable robust stability, dynamic dissipative compensators can be used. The main characteristic of all dissipative controllers is that they do not rely on the knowledge of the design model to ensure stability, although they use it to obtain the best possible performance. An n_c-order (two-level) dynamic dissipative controller is given by:

$$\dot{\mathbf{x}}_c = \mathbf{A}_c\mathbf{x}_c + \mathbf{B}_c\mathbf{y}_r \tag{10}$$

$$\mathbf{u}_c = -\mathbf{G}\mathbf{x}_c - \mathbf{G}_r\mathbf{y}_r - \mathbf{G}_p\mathbf{y}_p \tag{11}$$

where $\mathbf{A}_c, \mathbf{B}_c$, and $\mathbf{G}$ are the compensator system, input, and output matrices, respectively, and $\mathbf{G}_r$ and

$\mathbf{G}_p$ are symmetric, positive-definite rate gain and position gain matrices. Furthermore, $\mathbf{A}_c$ is strictly Hurwitz, and the Kalman-Yacubovich relations hold (ref. 17):

$$\mathbf{A}_c^T\mathbf{P} + \mathbf{P}\mathbf{A}_c = -\mathbf{Q} \tag{12}$$

$$\mathbf{G} = \mathbf{B}_c^T\mathbf{P} \tag{13}$$

where $\mathbf{P} = \mathbf{P}^T > 0$ and $\mathbf{Q} = \mathbf{Q}^T \geq 0$.

Equations (10)–(13) represent a two-level controller wherein the inner loop consists of static position-plus-rate feedback and the outer loop consists of a dynamic compensator. This controller assures robust asymptotic stability regardless of unmodeled structural dynamics or parametric uncertainties (refs. 5 and 16). In the absence of zero-frequency rigid-body modes (e.g., for a ground-based experiment), $\mathbf{G}_p$ and $\mathbf{G}_r$ can be null matrices without destroying the robust asymptotic stability; that is, the inner loop is not required. Further results for systems with zero-frequency modes are given in the appendix. As with the static dissipative controller, this control law has been proven to give guaranteed closed-loop stability despite unmodeled elastic modes and parameter errors. However, robust stability is generally not guaranteed if the actuator dynamics, nonlinearities, and time delays are present or if digital implementation is used. Also as with the static dissipative controller—for practical space implementation, rate measurements may be obtained from rate gyros and attitude measurements may be provided by star sensors. However, if linear velocity is required (e.g., in the case of ground-based experiments), velocity signals can be obtained by integrating accelerometer signals with the aid of washout filters to asymptotically remove the accelerometer bias. The inclusion of washout filters would, however, hinder the dissipativity of this control design.

Optimization-Based CSI Design

The methodology employed in this study uses optimization techniques to integrate the separate disciplines of control and structural design. Fundamentally, the integrated design goals and requirements are formulated as a nonlinear programming problem wherein selected control-structure design variables are chosen, subject to structural and performance constraints, to optimize an objective function whose construction captures the essence of the integrated design problem. It is felt that this approach takes advantage of the highly-developed optimization technology in both the controls and structures fields and provides the designer an opportunity to obtain nonintuitive results.

Nominally, an initial structure-control configuration defines a set of design variables that are available for modification. Typical controller design variables are size and location of sensors and actuators, and elements of dynamic compensator system matrices. Structural design parameters could be the dimensions of structural members along with mass and densities of materials. An example of a realistic integrated design problem would be, for some given input or maneuver, to design a spacecraft that provides the best possible reductions in dynamic response amplitude (below the amplitudes of a nominal spacecraft) with no increase in structural mass or control system energy requirements. As indicated by the preceding examples, most integrated design objectives and constraints can be expected to be dependent functions of the design variables that are obtained as the outputs of some separately developed computer control synthesis (ref. 18) or structural analysis packages (ref. 19). Integrated design is then a computationally intensive process requiring supercomputer technology.

A flowchart summarizing the process for optimization-based integrated design is given in figure 2. A user-provided executive program drives an optimization module that, at each stage, (1) uses the current values of the design variables to compute the objective function and constraints, (2) evaluates the objective function and constraints for optimality and feasibility, and (3) if necessary, generates a new set of design variables defining a structure-control configuration with better integrated-design characteristics. Aspects of the computer implementation of this process are discussed in reference 20.

A version of the integrated design software tool CSI-DESIGN, which is under development at the LaRC, was used to perform the numerical studies reported herein. CSI-DESIGN is intended for research purposes and is composed of public domain software. It uses in-core data transfer and is ultimately limited in the size of problems it can successfully treat. The package has linked control, structural, and optimization modules as shown in figure 2. The control compensator models used in this study were static and dynamic dissipative. The benefits and motivation for using this control strategy for the control of flexible structures are discussed in the appendix. A description of the contents of the CSI-DESIGN structural module may be found in reference 20. Integrated optimization was performed with a four-processor Alliant FX/80 digital computer that used the Automated Design Synthesis (ADS) software (ref. 21). The interior penalty function method of ADS was used to solve the nonlinear programming problems.

In this method, the constrained optimization problem is transformed into an unconstrained problem through creation of a pseudo-objective function that is the sum of the original objective function and an imposed penalty function, which is a function of the constraints (ref. 22). The Reverse-Cuthill-McKee algorithm for minimizing the bandwidth of the banded stiffness and mass matrices was used to reduce computational requirements (ref. 23). Additionally, analytical expressions for eigenvalue and eigenvector sensitivity (with respect to the structural design variables) (ref. 24) were used in the integrated design process to approximate the eigenvalues and eigenvectors at design points that are in the neighborhood of the nominal design point. This approximation was in the form of a first-order Taylor series approximation and resulted in substantial computational savings because it removes the need for costly computation of structural eigenvalues and eigenvectors at many of the optimization moves.

Integrated Design of the EPS Model

The Earth pointing system (EPS), a generic model of the geostationary platform is a multiuser concept and consists of a 10-bay, 30-m-long truss structure with two radial rib antennas (7.5 m and 15 m diameter) at the ends (fig. 3). All the members (i.e., constituting the truss, the antennas, and the antenna supports) are assumed to be hollow tubes with circular cross sections and thicknesses of 1.59 mm. The antennas are fixed with respect to the truss, so the problem is that of controlling the pointing and vibration of the entire structure. It is assumed that a three-axis control moment gyro (CMG) and collocated attitude and rate sensors, located at the center-of-mass of the structure, are used for accomplishing the control. No sensor and actuator dynamics are considered. The modal frequencies for the first 10 flexible modes are given in table 1. The first flexible mode had a frequency of 0.58 Hz, corresponding to a mode of the large antenna support structure, and the first flexible mode of the truss structure (mode 7) had a frequency of about 6.6 Hz. A design model consisting of three rigid-body modes and the first 10 flexible modes of the structure was used in the design process. An open-loop modal damping ratio of 0.5 percent was assumed for the flexible modes.

The integrated design problem was formulated as a single-objective optimization problem. The structural design variables used were outer diameters of the truss and antenna support members with the thicknesses fixed. In particular, the truss was divided into three sections shown in figure 3, and the outer diameters of the longerons, battens, and diagonals within each section constituted nine structural design variables. Two additional structural design variables were the outer diameters of the support members for the two antennas, thus constituting a total of 11 structural design variables. The number of control design variables varied and depended on the type of controller used. For the static dissipative design, the elements of the Cholesky factorization matrices of the positive-definite position and rate gain matrices $\mathbf{G}_p$ and $\mathbf{G}_r$ are chosen as design variables:

$$\left.\begin{aligned} \mathbf{G}_p &= \mathbf{L}_p\mathbf{L}_p^T \\ \mathbf{G}_r &= \mathbf{L}_r\mathbf{L}_r^T \end{aligned}\right\} \tag{14}$$

In dynamic dissipative designs, the elements of the compensator matrices $\mathbf{A}_c$ and $\mathbf{B}_c$, the elements of weighting matrix $\mathbf{Q}$, and the elements of the Cholesky factorization matrices $\mathbf{L}_p$ and $\mathbf{L}_r$ are used as design variables. Within this configuration, the following two design problems are considered.

Design Problem I

The system configuration for the first design problem is illustrated in the block diagram shown in figure 4. Here, white-noise disturbances of unit intensity are applied to the structure at the same locations as the control inputs, and no disturbances at the outputs are considered. The system equations are given as

$$\dot{\mathbf{z}} = \mathbf{A}\mathbf{z} + \mathbf{B}\mathbf{u} + \mathbf{B}\mathbf{w} \tag{15}$$

$$\left.\begin{aligned} \mathbf{y}_p &= \mathbf{C}_p\mathbf{z} \\ \mathbf{y}_r &= \mathbf{C}_r\mathbf{z} \\ \mathbf{y}_{\text{per}} \equiv \mathbf{e} &= \mathbf{C}_{\text{per}}\mathbf{z} \end{aligned}\right\} \tag{16}$$

In this design problem, the closed-loop performance measure is the steady-state rms pointing error vector $\mathbf{e}$ at the large antenna due to white-noise disturbance of unit intensity at the inputs. To achieve a realistic design, constraints are placed on the steady-state average control power and the total structural mass. Additional side constraints are placed on the structural design variables for safety and practicality reasons. Lower bounds are placed on these variables to satisfy structural integrity requirements against buckling and stress failures. On the other hand, upper bounds are placed on these variables to accommodate manufacturing limitations. The first design problem is described as follows.

Minimize the steady-state rms pointing error at the large antenna

$$J = \lim_{t\to\infty}\left(\text{Tr}\left\{E\left[\mathbf{e}(t)\,\mathbf{e}^T(t)\right]\right\}\right)^{1/2} \tag{17}$$

with respect to the tube outer diameters $d_i (i = 1, 2, \ldots, 11)$, and the elements of $\mathbf{L}_p$ and $\mathbf{L}_r$ (where $\mathbf{L}_p$ and $\mathbf{L}_r$ are 3×3 lower-triangular Cholesky factors of $\mathbf{G}_p$ and $\mathbf{G}_r$ given in eq. (14)), subject to the constraints:

$$\lim_{t \to \infty} \left(\mathrm{Tr} \left\{ E \left[\mathbf{u}(t) \, \mathbf{u}^T(t) \right] \right\} \right) \leq P_{\max} \tag{18}$$

$$M_{\mathrm{str}} \leq M_{\max} \tag{19}$$

$$d_{\min} \leq d_i \leq d_{\max} \tag{20}$$

where $\mathbf{e}$ is the 3×1 attitude vector at the large antenna, Tr( ) denotes trace of ( ), E( ) represents expected value of ( ), and M_{str} denotes the structural mass. The subscripts min and max define the range of allowable values.

The steady-state covariance of the pointing error vector $\mathbf{P_e}$ is computed from the steady-state covariance of the state vector; that is,

$$\mathbf{P_e} \equiv \lim_{t \to \infty} \mathrm{Tr} \left[E \left(\mathbf{e} \mathbf{e}^T \right) \right] = \mathrm{Tr} \left(\mathbf{C}_{\mathrm{per}} \mathbf{P_z} \mathbf{C}_{\mathrm{per}}^T \right) \tag{21}$$

where $\mathbf{P_z} = \lim_{t \to \infty} E(\mathbf{z}\mathbf{z}^T)$ denotes the steady-state covariance of the state that is determined from the solution of the following Liapunov equation (ref. 25):

$$\mathbf{A}_{\mathrm{cl}} \mathbf{P_z} + \mathbf{P_z} \mathbf{A}_{\mathrm{cl}}^T = -\mathbf{B}\mathbf{B}^T \tag{22}$$

in which $\mathbf{A}_{\mathrm{cl}}$ is the closed-loop state matrix and $\mathbf{B}$ is the control (input) influence matrix.

The results for this design problem are summarized in table 2. An initial control design was first obtained for the nominal structure. Using a pole placement technique, a decoupled controller was designed to provide adequate performance for each of the three rigid-body modes, with no consideration given to the flexible modes. That is, the static-dissipative control gain matrices were diagonal, with elements chosen to give satisfactory closed-loop frequency and damping for the rigid-body dynamics and to maintain the RMS pointing error within the required tolerance. The nominal structural mass was 442.04 kg and the actuator mass was assumed constant at 150 kg.

With the average control power $P_{\max}$ constrained at 3 N^2-m^2, the initial design gave an rms pointing error of 73.6 μrad. The conventional design approach was then followed, wherein the control gains (12 elements of the two Cholesky factors $\mathbf{L}_p$ and $\mathbf{L}_r$) were optimized for the fixed nominal structure. This control-optimized design yielded an rms pointing error of 26.8 μrad. Next, an integrated design was performed, wherein both the structural and control design variables were allowed to change simultaneously. This integrated design resulted in an rms error of 16.8 μrad, which represented a 37-percent reduction over the conventional design. The structural mass was slightly lower than the nominal design. The upper and lower bound values, initial values, and the optimal values of the structural design variables are summarized in table 3 and figure 5. The integrated design redistributed the structural mass from the battens and diagonals of the last two sections of the main bus (closest to the small antenna) and small antenna support members to the large antenna support members and the section of the main bus closest to the large antenna, thus increasing the stiffness of these sections. This behavioral trend may be attributed to a trade-off between structural controllability and observability and its excitability by disturbances. In other words, the stiffness (or flexibility) of the structure is redistributed to establish a balance between the ability of the control system to fine-point the structure efficiently and the ability of the structure to reject disturbances.

The modal frequencies of the first 10 flexible modes of the redesigned EPS structure (redesigned through the integrated design process) are presented in table 4. The data indicate that the first three frequencies (modes 1–3) associated with the small antenna support structure have been reduced substantially, mainly because the pointing performance of the small antenna was not included in the performance metric. On the other hand, the frequency of the modes associated with the large antenna support structure has increased considerably (for example, the first modal frequency increased from 0.58 Hz (table 1) to 2.75 Hz (table 4)), thus making the large antenna and support structure less sensitive to disturbances at the inputs or the outputs. At the same time, the first flexible frequency of the main truss (mode 7) decreased from about 6.6 Hz (table 1) to about 6.0 Hz (table 4), making the main truss more sensitive to disturbances but more controllable (observable). The elements of the 3×3 lower triangular Cholesky factorization matrices $\mathbf{L}_p$ and $\mathbf{L}_r$ are given in table 5 for the nominal controller design, the control-optimized design, and the integrated controls-structures design. The attitude and rate gain matrices may be computed from the Cholesky matrices by using equation (14).

To evaluate the effect of varying the actuator mass in the integrated design process, the actuator mass was allowed to vary by relating it to the infinity

norms of the gain matrices (a worst-case scenario); that is,

$$M_{\text{act}} = \alpha \left|\mathbf{u}\right|_\infty \equiv \alpha \left(\left|\mathbf{G}_r\right|_\infty \left|\mathbf{y}_r\right|_\infty + \left|\mathbf{G}_p\right|_\infty \left|\mathbf{y}_p\right|_\infty \right) \quad (23)$$

in which α is a constant scalar taken to be 1.005 and $|\ |_\infty$ denotes the infinity norm of $|\ |$. It is noted that $|\mathbf{y}_p|_\infty$ and $|\mathbf{y}_r|_\infty$ were assumed fixed a priori to be 0.1 rad and 0.1 rad/sec, respectively. For this case, the actuator mass increased from 150 kg to 298.7 kg, whereas the rms pointing error and the structural mass were essentially unaffected, which is because the structure is rather stiff and is not affected by small masses.

Design Problem II

The system configuration for the second design problem is illustrated in the block diagram shown in figure 6. Here, the attitude and rate sensors are assumed to be polluted with noise modeled as zero-mean, white-noise processes. Furthermore, no disturbances at the inputs are considered. With this configuration, the system equations become

$$\dot{\mathbf{z}} = \mathbf{A}\mathbf{z} + \mathbf{B}\mathbf{u} \quad (24)$$

$$\left.\begin{aligned} \mathbf{y}_p &= \mathbf{C}_p\mathbf{z} + \mathbf{S}_p\mathbf{v}_p \\ \mathbf{y}_r &= \mathbf{C}_r\mathbf{z} + \mathbf{S}_r\mathbf{v}_r \\ \mathbf{y}_{\text{per}} &\equiv \mathbf{e} = \mathbf{C}_{\text{per}}\mathbf{z} \end{aligned}\right\} \quad (25)$$

where $\mathbf{v}_p$ and $\mathbf{v}_r$ denote the attitude and rate sensors noise vectors, and $\mathbf{e}$ represents the rms pointing error vector at the large antenna. In this design problem, a dual-objective formulation is pursued, wherein both the total mass (structure plus actuator) and a measure of the closed-loop performance are optimized. The closed-loop performance measure is chosen as the sum of the time constants of the closed-loop eigenvalues (the reciprocals of the absolute value of the real part of the closed-loop eigenvalues), which represents a measure of the transient performance of the system (i.e., the smaller the time constants are, the faster the system dissipates transient disturbances). The closed-loop or controlled performance $\mathrm{P_c}$ is the inverse of the sum of the time constants of the system, such that

$$\mathrm{P_c} = \frac{1}{\sum \left[\frac{1}{|\mathrm{Re}(\lambda_i)|} \right]} \quad (26)$$

Now, to minimize the total mass and maximize the closed-loop performance, an objective function J consisting of a convex combination of the total mass and the inverse of $\mathrm{P_c}$ is minimized. The design problem is to minimize

$$J = \beta \frac{M_{\text{str}} + M_{\text{act}}}{M^o_{\text{str}} + M^o_{\text{act}}} + (1-\beta)\,\frac{1/\mathrm{P_c}}{1/\mathrm{P^o_c}} \quad (27)$$

with respect to structural and/or control design variables, subject to a constraint on $\mathbf{e}$

$$\lim_{t\to\infty} \left(\mathrm{Tr} \left\{ E\left[\mathbf{e}\,(t)\, \mathbf{e}^T\,(t) \right] \right\} \right) \le e_{\max} \quad (28)$$

as well as side constraints on structural member sizes

$$d_{\min} \le d_i \le d_{\max} \quad (29)$$

Note that both the mass term and the term for the controlled performance in equation (27) are normalized with respect to their corresponding initial values. In equation (27), M_{str} and M_{act} denote the structural (truss) mass and the actuator mass, and the superscript o denotes the initial value of the corresponding variable. The covariance of $\mathbf{e}$ is computed from the steady-state covariance of the state vector; that is,

$$\mathbf{P_e} \equiv \lim_{t\to\infty} \mathrm{Tr}\left[E\left(\mathbf{e}\mathbf{e}^T \right) \right] = \mathrm{Tr}\left(\mathbf{C}_{\text{per}} \mathbf{P_z} \mathbf{C}^T_{\text{per}} \right) \quad (30)$$

where $\mathbf{P_z} = \lim_{t\to\infty} E(\mathbf{z}\mathbf{z}^T)$ denotes the closed-loop steady-state covariance of the state that is determined from the solution of the following Liapunov equation (ref. 25):

$$\mathbf{A}_{\text{cl}}\mathbf{P_z} + \mathbf{P_z}\mathbf{A}^T_{\text{cl}} = -\mathbf{B}\mathbf{G}_p\mathbf{W}_p\mathbf{G}^T_p\mathbf{B}^T - \mathbf{B}\mathbf{G}_r\mathbf{W}_r\mathbf{G}^T_r\mathbf{B}^T \quad (31)$$

in which the attitude measurement noise intensity matrix, $\mathbf{W}_p = E(\mathbf{v}_p\mathbf{v}^T_p)$, and the rate measurement noise intensity matrix, $\mathbf{W}_r = E(\mathbf{v}_r\mathbf{v}^T_r)$, are assumed to be diagonal (i.e., $\mathbf{W}_p = \mathbf{I}_{3\times3}$ (arcsec)^2 and $\mathbf{W}_r = 2\times\mathbf{I}_{3\times3}$ (arcsec/sec)^2). The pointing tolerance $e_{\max}$ in equation (28) is taken as 11 μrad.

The parameter β allows for a trade-off between the two objectives. As β is varied from one to zero, more emphasis is placed on the closed-loop performance and less on the total mass or the cost. Furthermore, to satisfy certain fine-pointing requirements, an upper bound constraint is placed on the rms error at the large antenna due to white measurement noise in the attitude and rate sensors. Additional side constraints are also placed on the structural design variables for safety and practicality concerns. Figures 7(a)–(d) show, respectively, the behavior (normalized relative to the nominal design) of the objective function J, controlled performance (a measure

of transient performance), structural mass, and actuator mass as a function of the trade-off parameter β. As β approaches zero, the design becomes *performance* or *control* dominated, as evidenced by the sharp increase in the controlled performance (fig. 7(b)) and the substantial increases in the structural and actuator masses (figs. 7(c) and (d)). On the other hand, as β approaches one, the controlled performance diminishes considerably, and the structural mass and actuator mass decrease, giving a *mass* or *cost-dominated* design.

One may use these trade-off results to obtain a design that gives a good controlled performance with acceptable cost levels by choosing a right value for β. For example, at $\beta = 0.50$, table 6 gives the corresponding integrated design with a control-optimized (conventional) design. An initial design to achieve good rigid-body performance (same as design problem I) was first obtained. This design required an actuator mass of about 171 kg (computed from eq. (23)), which along with the nominal structural mass of 442.04 kg and payload mass of 5168 kg, resulted in a total spacecraft mass of 5781.04 kg. The controlled performance measure P_c was about 0.003. Then, a control-optimized design was performed by optimizing the control variables only. This design resulted in a 44-percent increase in the control performance, but also increased the total mass by 1 percent (57.17 kg). An integrated design was next carried out, which resulted in a 234-percent increase in the control performance along with lower total mass over the initial design (6 percent less than the total mass of the control-optimized design, or about 353 kg). Integrated design reduced the structural mass by 53 percent and decreased the actuator mass by 24 percent.

The optimization data and results for the structural design variables are given in table 7 and figure 8. It is observed that the structural mass was reduced and redistributed (i.e., mass was taken from the main bus structure and was added to the antenna support members). In other words, most of the longerons, battens, and diagonals of the main bus structure were reduced to lower bound values, while the antenna support members increased drastically in size. The open-loop modal frequencies of the redesigned EPS structure (obtained through integrated design process) are presented in table 8, where it is seen that the first flexible frequency corresponding to the large antenna support structure increased to near 1.8 Hz, with a reduction of truss flexible frequencies by as much as 50 percent at the higher end of the spectrum. In this configuration, the antennas are less susceptible to disturbances at the inputs or the outputs, whereas the overall structure has become more controllable (observable).

The closed-loop eigenvalues are presented in figures 9–11 for the nominal design, the control-optimized design, and the integrated controls-structures design, respectively. These figures indicate that integrated design is more effective than the conventional design in moving the closed-loop eigenvalues of the system farther into the left-half plane (such that the system can dissipate transient disturbances faster), thus clearly demonstrating the advantage of the integrated design. Also, the Cholesky factorization matrices $\mathbf{L}_p$ and $\mathbf{L}_r$ (associated with the attitude and rate gain matrices) are given in table 9 for the nominal design, the control-optimized design, and the integrated design.

Summarizing the results obtained from design problems I and II, both clearly show the advantage of integrated design over the conventional approach in that the integrated design produces a better overall design. The main advantage of integrated design is its ability to obtain a better overall design and not necessarily just a reduction of the total mass. Moreover, a comparison of the behavioral trends of the structural design variables for the first and second design problems indicates that such trends could vary considerably depending on the design objectives and constraints of the integrated design problem.

Integrated Design of the CSI Evolutionary Model

This section considers the application of the integrated design methodology to the CSI Evolutionary Model. The discussion on the application is in English units to be consistent with the formal model of the structure (ref. 14). The Phase-Zero Evolutionary Model, shown in figure 12, basically consists of a 62-bay central truss (each bay 10 in. long), two vertical towers, and two horizontal booms. Using two cables as shown, the structure is suspended from the ceiling (about 840 in. above the main truss). A laser source is mounted at the top of one of the towers, and a reflector with a mirrored surface is mounted on the other tower. The laser beam is reflected by the mirrored surface onto a detector surface 660 in. above the reflector. Eight proportional bidirectional gas thrusters, with maximum output force of 4.4 lb each, provide the input actuation, and collocated servo accelerometers provide output measurements. The finite element model of the system has 3216 degrees of freedom; therefore, the bulk of the computational effort is required for the solution of the structural eigenvalue problem of that size.

The design model consisted of the first 20 modes of the structure, including 6 suspension modes (i.e., modes due to the suspension of the structure and gravity) and 14 flexible modes. A modal damping ratio of 0.1 percent was assumed. The first 20 modes of the nominal Phase-0 Model are presented in table 10. The first six modes that range from 0.12 Hz to 1.16 Hz are the suspension modes (or non-zero-frequency–rigid-body modes). The first two bending modes (lateral and vertical) and the first torsional modes of the structure are modes 7, 8, and 9. The system configuration for this design problem is illustrated in block diagram shown in figure 13. Here, white-noise disturbances of unit intensity are applied to the structure at the same locations as the control inputs, and no disturbances at the outputs are considered. With no appreciable sensor and actuator dynamics considered, the system equations are written as

$$\dot{\mathbf{z}} = \mathbf{A}\mathbf{z} + \mathbf{B}\mathbf{u} + \mathbf{B}\mathbf{w} \tag{32}$$

$$\left.\begin{aligned} \mathbf{y}_r &= \mathbf{C}_r\mathbf{z} \\ \mathbf{y}_{\text{per}} \equiv \mathbf{e} &= \mathbf{C}_p\mathbf{z} \end{aligned}\right\} \tag{33}$$

where the performance vector $\mathbf{y}_{\text{per}}$ is an 8×1 vector corresponding to the displacements at the eight accelerometer locations. Here, only velocity measurements are used for feedback, and they are obtained by integrating the accelerometer signals with the aid of wash-out filters. It is noted that position feedback is not necessary for asymptotic stability because the structure is open-loop stable.

To perform the integrated design, the structure was divided into seven sections (see fig. 12), three sections in the main bus, and one section each for the two horizontal booms and the two vertical towers. Three structural design variables were used in each section, namely, outer diameters of the longerons, the battens, and the diagonals, making a total of 21 structural design variables. The design was posed in the form of a nonlinear optimization problem, wherein the steady-state average control power in the presence of a white-noise input disturbance with unit intensity (i.e., Standard deviation intensity = 1 lbf) is minimized, with the steady-state rms position error vector at the eight accelerometer locations and total mass constrained to required values. That is, the problem solved was:

Minimize

$$\lim_{t\to\infty} \text{Tr}\left[E\left\{\mathbf{u}(t)\,\mathbf{u}^T(t)\right\}\right] \tag{34}$$

subject to

$$\lim_{t\to\infty} \left(\text{Tr}\left\{E\left[\mathbf{e}(t)\;\mathbf{e}^T(t)\right]\right\}\right)^{\frac{1}{2}} \leq e_{\max} \tag{35}$$

and a constraint on the total mass

$$M_{\text{tot}} \leq M_{\max} \tag{36}$$

Here, $e_{\max}$ was taken to be 1.7 in. and $M_{\max}$ was chosen equal to the total mass of the nominal Phase-0 structure at 2.0 lb-sec^2/in.

Static Dissipative Controller

As mentioned earlier, only velocity measurements are used for feedback, which are obtained by processing the accelerometer outputs. Thus, the static dissipative controller is given by

$$\mathbf{u} = -\mathbf{G}_r\mathbf{y}_r \tag{37}$$

Here, the rate gain matrix was an 8×8 diagonal matrix (i.e., eight control design variables, along with the 21 structural design variables, resulted in a total of 29 design variables for the design optimization).

The results of the design optimization are summarized in table 11. A conventional or control-optimized design was first performed (with the structural design fixed at the nominal values), which required an average steady-state control power of 19.34 lb^2.

Next, an integrated design was performed, wherein the average control power was minimized with respect to both control and structural design variables. The results (table 11) indicate an average control power of 11.41 lb^2, a reduction of about 40 percent in the average control power over the conventional design. The initial and final values of the structural design variables, along with the corresponding lower bound and upper bound values, are presented in table 12 and figure 14. Keeping in mind that the tube diameters of the nominal CSI Evolutionary Model structure are 0.367 in. for the longerons and battens and 0.349 in. for the diagonal, it is observed from table 12 and figure 14 that sections 1 and 2 of the main bus (farthest away from the reflector) and the laser tower are considerably stiffened, whereas the horizontal booms and the reflector tower became more flexible, partly to satisfy the mass constraint. Generally, in those sections that showed an increase in stiffness, the longerons increased in size more than the diagonals and the battens, because they were most effective in changing the stiffness of a section.

The trends in table 12 may be attributed to a trade-off between structural controllability, observability, and excitability. The areas near the sources of disturbance (actuator locations) were stiffened in order to reduce the sensitivity of the structure to external disturbances at those locations, while ensuring that no appreciable loss of controllability and/or observability occurred (as observed from the transient controlled performance values in table 11). The small reduction in the transient controlled performance of the integrated design over the conventional design in table 11 is mainly because no measure of the transient performance was included in the optimization process. Moreover, although the transient controlled performance was lower in the integrated design case, it is still quite acceptable. The modal frequencies of the first 20 modes of the redesigned Phase-0 structure (redesigned through the integrated design process) are presented in table 13. These frequencies indicate that the first six frequencies associated with the suspended structure have not been changed significantly, mainly because the changes in the structure can affect these frequencies only through changing the location of the center of mass of the structure and not directly as is the case for the flexible modes. On the other hand, the frequencies of the flexible modes, particularly the second and third flexible modes, have increased considerably (as much as 40 percent). The second flexible mode frequency increased from 1.68 Hz to 2.33 Hz (mode 8 in table 13) and the third flexible mode frequency from 2.08 Hz to 2.65 Hz (mode 9 in table 13), making these modes and the structure less sensitive to disturbances at the inputs. The diagonal elements of the rate gain matrix are given in table 14 for the control-optimized design and the integrated controls-structures design.

Dynamic Dissipative Controller

The next two designs that were performed for the CSI Evolutionary Model were conventional (control-optimized) and integrated designs with a dynamic dissipative controller. Because the system has no zero-frequency modes, $\mathbf{G}_p$ and $\mathbf{G}_r$ were taken to be zero. The dynamic dissipative controller represented by equations (10) and (11) was used with block-diagonal compensator state matrix $\mathbf{A}_c$ (consisting of eight second-order blocks) and compensator input influence matrix $\mathbf{B}_c$ as follows:

$$\mathbf{A}_c = \begin{bmatrix} \mathbf{A}_{c1} & 0 & \dots & 0 \\ 0 & \mathbf{A}_{c2} & \dots & 0 \\ \vdots & \vdots & \ddots & \vdots \\ 0 & 0 & \dots & \mathbf{A}_{c8} \end{bmatrix} \tag{38}$$

$$\mathbf{B}_c = \begin{bmatrix} \mathbf{B}_{c1} & 0 & \dots & 0 \\ 0 & \mathbf{B}_{c1} & \dots & 0 \\ \vdots & \vdots & \ddots & \vdots \\ 0 & 0 & \dots & \mathbf{B}_{c8} \end{bmatrix} \tag{39}$$

where $\mathbf{A}_{ci}$ and $\mathbf{B}_{ci}$ $(i = 1, 2, \dots, 8)$ are, respectively, 2×2 matrices and 2×1 vectors, defined as

$$\left.\begin{aligned} \mathbf{A}_{ci} &= \begin{bmatrix} 0 & 1 \\ -\alpha_i & -\beta_i \end{bmatrix} \\ \mathbf{B}_{ci} &= \begin{bmatrix} 0 \\ 1 \end{bmatrix} \end{aligned}\right\} \tag{40}$$

Furthermore, the weighting matrix $\mathbf{Q}$ in equation (12) is assumed to be diagonal; that is,

$$\mathbf{Q} = \text{Diag}\,(q_1, q_2, \dots, q_{16}) \tag{41}$$

Here, the scalar variables α_i, β_i $(i = 1, 2, \dots, 8)$, and q_j $(j = 1, 2, \dots, 16)$ were chosen for the control design variables. Thus, the number of control design variables was 32, making the total number of design variables 53. Table 15 shows the results of the designs with the dynamic dissipative controller. The conventional design reduces the control power by over 50 percent (to 8.31 lb^2), compared with the static dissipative case. The integrated design reduces the average control power by approximately another 30 percent (over the conventional design) to 5.91 lb^2. Table 15 also indicates that the transient controlled performance is slightly lower for the integrated design case. Similar to the static dissipative design, this reduction in performance is because the optimization process did not include any measure of transient performance. Moreover, although tables 11 and 15 show that the transient controlled performance of the dynamic dissipative design was quite lower than the static dissipative design, one should keep in mind that in the dynamic dissipative design, this performance measure includes contributions from the compensator poles, and thus it is not readily comparable with the static dissipative values.

The optimization data and results for the structural design variables are summarized in table 16 and figure 15. The trends are quite similar to the static dissipative design given in table 12. In fact, the two optimal structures are within 20 percent of each other (i.e., the structure that is optimal for the static dissipative design is also optimal for the dynamic dissipative design). The modal frequencies of the optimal structure for the dynamic dissipative design are summarized in table 17. These frequencies are also close (within 5 percent) to their corresponding values

for the static dissipative design. Finally, the singular value plots for the input-to-output transfer functions of the dynamic dissipative compensator are presented in figures 16(a)–(h) for the control-optimized design and the integrated controls-structures design. The singular value plots for the control-optimized design and the integrated design are somewhat similar except for input/output channel nos. 1 and 7 (see figs. 16(a) and (g)), where considerable reduction in the singular values, mainly in the lower end of the frequency spectrum, and increase in the bandwidth are observed in the integrated design case over the conventional design. The elements of the compensator state matrix $\mathbf{A}_c$ are given in table 18 for the control-optimized design and the integrated controls-structures design. Also, the elements of the weighting matrix $\mathbf{Q}$ are presented in table 19 for both designs.

The results obtained for both the static and dynamic dissipative controllers clearly show that integrated controls-structures design methodology can yield an overall design that is substantially superior than the conventional sequential design scenario.

Concluding Remarks

An optimization-based approach has been developed for performing integrated controls-structures design of a class of flexible spacecraft. The approach formulates the problem as a constrained optimization problem, wherein the set of design variables consists of both control and structural design variables. The approach uses static and dynamic dissipative control laws, which provide robust stability in the presence of parametric and nonparametric uncertainties in the model. The approach was demonstrated by application to integrated designs of a generic model of a space platform concept, as well as to a model of the Controls-Structures Interaction (CSI) program's Evolutionary Model, which is a ground-based experimental testbed developed and constructed at Langley Research Center.

The numerical results obtained indicate that the integrated design approach can yield substantially superior spacecraft design as compared with the traditional sequential design approach. For example, a 40-percent reduction in the pointing error is observed along with a slight reduction in mass, or an almost twofold increase in the controlled performance is indicated with more than a 5-percent reduction in the overall mass of the spacecraft (a reduction of hundreds of kilograms). Furthermore, the automated nature of the integrated design approach can accommodate a wide variety of design specifications and requirements. A practical software tool (CSI-DESIGN) is being developed for performing integrated designs. Research is presently in progress for incorporating other types of control methods (such as H_2 or H_∞) into the integrated design process. Future plans also include hardware validation of the integrated design approach by constructing a laboratory test article based on the redesigned CSI Evolutionary Model and comparing the performance of the redesigned structure with the original CSI Evolutionary Model.

NASA Langley Research Center
Hampton, VA 23681-0001
October 14, 1992

Appendix

Dissipative Controllers

This appendix briefly presents the main results concerning dissipative controllers for flexible structures. Dissipative controllers use the passivity properties of the system that result from the use of collocated and compatible actuators and sensors, such as torque actuators and attitude and rate sensors or force actuators and position and velocity sensors. In general, dissipative controllers are designed to control both rigid and elastic modes. In certain cases, the zero-frequency rigid modes may not be present. This may occur, for example, when paired torquers are used in a balanced configuration to control only the elastic motion (ref. 4) or in the case of ground-based test articles. In such cases, no position feedback is required; only velocity feedback is sufficient to accomplish robust stability, and the dissipative compensator degenerates to a positivity controller. In the following, both the static and dynamic dissipative controllers are discussed. The concepts and the underlying theory are based largely on the original work of Popov (ref. 26).

Static Dissipative Controllers

The constant-gain or static dissipative control law is given by:

$$\mathbf{u} = -\mathbf{G}_p\mathbf{y}_p - \mathbf{G}_r\mathbf{y}_r \qquad \text{(A1)}$$

where $\mathbf{G}_p$ and $\mathbf{G}_r$ are $m \times m$ symmetric, positive-definite, position and rate gain matrices, and $\mathbf{y}_p$ and $\mathbf{y}_r$ represent the $m \times 1$ position and rate measurement vectors. This control law is known to give guaranteed asymptotic stability of the entire system consisting of both rigid and flexible modes regardless of unmodeled elastic modes or parameter uncertainties. (It was also shown in ref. 4 that stability is maintained even if small imprecision exists in the collocation of the actuators and sensors.) Furthermore, if $\mathbf{G}_p$ and $\mathbf{G}_r$ are diagonal, this robust stability property is carried over in the presence of:

(1) Monotonically increasing actuator nonlinearities, rate sensor nonlinearities belonging to the $[0, \infty)$ sector, and position sensor nonlinearities belonging to the $(0, \infty)$ sector (a single-valued function $\psi(\nu)$ is said to belong to the $(0, \infty)$ sector if $\psi(0) = 0$ and $\nu\psi(\nu) > 0$ for $\nu \neq 0$; ψ is said to belong to the $[0, \infty)$ sector if $\nu\psi(\nu) \geq 0$), and

(2) Stable actuator dynamics $g_a(s) = k/(s + a)$, provided that $g_p/g_r < a$, where g_p and g_r denote the appropriate diagonal elements of $\mathbf{G}_p$ and $\mathbf{G}_r$. A possible drawback of these controllers is that the performance can be limited because of the structure of the controller. The matrices $\mathbf{G}_p$ and $\mathbf{G}_r$ can be designed to minimize a quadratic performance function or to obtain closed-loop eigenvalues close to the desired locations in the least-square sense (ref. 4).

When the zero-frequency modes are absent, $\mathbf{G}_p$ can be zero, and $\mathbf{G}_r = \mathbf{G}_r^T > 0$ is sufficient for asymptotic stability. Furthermore, the closed-loop system is robust to $[0, \infty)$-sector actuator and sensor nonlinearities and first-order actuator dynamics (ref. 4).

Dynamic Dissipative Controllers

To obtain better performance while still retaining the guaranteed robustness to unmodeled dynamics and parameter uncertainties, a class of dynamic dissipative controllers was considered. The case in which both zero-frequency rigid modes and flexible modes are present is considered first.

Assuming for simplicity that the plant has three (one per axis) torque actuators and collocated attitude and rate sensors, the 3×3 transfer function from the torque input to the attitude rate output is given by:

$$\boldsymbol{G}'(s) = \frac{\mathbf{J}^{-1}}{s} + \sum \frac{\boldsymbol{\Phi}_i \boldsymbol{\Phi}_i^T s}{s^2 + 2\rho_i\omega_i s + \omega_i^2} \qquad \text{(A2)}$$

where $\mathbf{J}$ is the moment-of-inertia matrix and $\boldsymbol{\Phi}_i, \rho_i$, and ω_i denote the rotational mode shape vector, damping ratio, and natural frequency of the ith structural mode. The transfer function $\boldsymbol{G}'(s)$ is positive real (PR), as defined as follows (ref. 27):

Definition

A rational matrix-valued function $\boldsymbol{T}(s)$ of the complex variable s is said to be PR if $\boldsymbol{T}(s)$ is real when s is real, and $\boldsymbol{T}(s) + \boldsymbol{T}^T(s^*) \geq 0$ for $\mathrm{Re}(s) \geq 0$, where * denotes the complex conjugate.

Scalar PR functions have a relative degree (i.e., the difference between the degrees of the denominator and numerator polynomials) of -1, 0, or 1 (ref. 28). It can also be shown that PR matrices have no transmission zeros or poles in the open right-half of the complex plane and that the poles on the imaginary axis are simple and have nonnegative definite residues. By applying the maximum modulus theorem, it can be shown that it is sufficient to check the positive semidefiniteness of $\boldsymbol{T}(s)$ only on

the imaginary axis ($s = j\omega, 0 \leq \omega < \infty$). Suppose $(\boldsymbol{A}, \boldsymbol{B}, \boldsymbol{C}, \boldsymbol{D})$ is an nth-order minimal realization of $\boldsymbol{T}(s)$. From reference 27, a necessary and sufficient condition for $\boldsymbol{T}(s)$ to be PR is that there exists an $n \times n$ symmetric positive-definite matrix $\mathbf{P}$ and matrices $\mathbf{W}$ and $\mathbf{L}$ such that

$$\left.\begin{aligned} \boldsymbol{A}^T\mathbf{P} + \mathbf{P}\boldsymbol{A} &= -\mathbf{L}\mathbf{L}^T \\ \boldsymbol{C} &= \boldsymbol{B}^T\mathbf{P} + \mathbf{W}^T\mathbf{L} \\ \mathbf{W}^T\mathbf{W} &= \boldsymbol{D} + \boldsymbol{D}^T \end{aligned}\right\} \tag{A3}$$

This result is generally known in the literature as the Kalman-Yacubovich lemma. A stronger concept along these lines is strictly positive-real (SPR) systems. However, there are several nonequivalent definitions of SPR, all of which require the system to have all poles in the open left half plane (ref. 29). For the purpose of this paper, we define a less restrictive class of strongly PR systems as follows:

Definition

A rational matrix-valued function $\boldsymbol{T}(s)$ of the complex variable s is said to be strongly PR if $\boldsymbol{T}(s)$ is real when s is real, and $\boldsymbol{T}(s) + \boldsymbol{T}^T(s^*) > 0$ for $\mathrm{Re}(s) \geq 0$.

The obvious difference between this definition and the definition of PR systems is that $\geq$ has been replaced by strict inequality. The difference between the strongly PR and SPR systems is that the latter have poles only in the open left half plane, whereas the former can have poles on the $j\omega$-axis.

The transfer function from $\mathbf{u}$ to $\mathbf{y}_p$ is given by:

$$\boldsymbol{G}(s) = \frac{\boldsymbol{G}'(s)}{s} \tag{A4}$$

It can be seen that $\boldsymbol{G}(s)$ is not PR. However, $\boldsymbol{G}'(s)$, the transfer function from $\mathbf{u}$ to $\mathbf{y}_r$, is PR.

Definition

The compensator $\boldsymbol{K}(s)$ is said to stabilize a plant $\boldsymbol{G}(s)$ if the closed-loop system consisting of stabilizable and detectable realizations of $\boldsymbol{K}$ and $\boldsymbol{G}$ in the standard feedback configuration is asymptotically stable (a.s.).

Suppose a controller $\boldsymbol{K}(s)$ is represented by the n_Kth-order minimal realization:

$$\dot{\mathbf{x}}_K = \mathbf{A}_K\mathbf{x}_K + \mathbf{B}_K\mathbf{y}_p \tag{A5}$$

$$\mathbf{y}_K = \mathbf{C}_K\mathbf{x}_K + \boldsymbol{D}_K\mathbf{y}_p \tag{A6}$$

The input to the plant is given by:

$$\mathbf{u} = -\mathbf{y}_K \tag{A7}$$

Define

$$\left.\begin{aligned} \mathbf{A}_\mathbf{z} &= \begin{bmatrix} \mathbf{A}_K & 0 \\ \mathbf{C}_K & 0 \end{bmatrix} \\ \mathbf{B}_\mathbf{z} &= \begin{bmatrix} \mathbf{B}_K \\ \boldsymbol{D}_K \end{bmatrix} \\ \mathbf{C}_\mathbf{z} &= [0 \quad \mathbf{I}_{3\times 3}] \end{aligned}\right\} \tag{A8}$$

We present the following stability result that was proved in reference 16.

Theorem 1

Suppose

(i) The matrix $\mathbf{A}_K$ is strictly Hurwitz

(ii) There exists an $(n_K + 3) \times (n_K + 3)$ matrix $\mathbf{P}_\mathbf{z} = \mathbf{P}_\mathbf{z}^T > 0$ such that

$$\mathbf{A}_\mathbf{z}^T\mathbf{P}_\mathbf{z} + \mathbf{P}_\mathbf{z}\mathbf{A}_\mathbf{z} = -\mathbf{Q}_\mathbf{z} = -\mathrm{diag}\left(\mathbf{L}_K^T\mathbf{L}_K, 0_{3\times 3}\right) \tag{A9}$$

where $\mathbf{L}_K$ is a $3 \times n$ matrix such that $(\mathbf{L}_K, \mathbf{A}_K)$ is observable, and $\mathbf{L}_K(s\mathbf{I} - \mathbf{A}_K)^{-1}\mathbf{B}_K$ has no transmission zeros in $\mathrm{Re}(s) \geq 0$

(iii) The matrix $\mathbf{C}_\mathbf{z}$ is defined as

$$\mathbf{C}_\mathbf{z} = \mathbf{B}_\mathbf{z}^T\mathbf{P}_\mathbf{z} \tag{A10}$$

(iv) The equation $\boldsymbol{K}(s) = \mathbf{C}_K(s\mathbf{I} - \mathbf{A}_K)^{-1}\mathbf{B}_K + \boldsymbol{D}_K$ has no transmission zeros at the origin.

Under these conditions, the controller $K(s)$ stabilizes $G(s)$.

Remark 1. In theorem 1, if $\mathbf{L}_K$ is an $n_K \times n_K$ nonsingular matrix, then the observability and minimum-phase properties in condition (ii) are satisfied and the closed-loop system is a.s.

Remark 2. The controller $\boldsymbol{K}$ stabilizes the full plant (i.e., the system consisting of the rigid modes, the elastic modes, and the compensator state vector $(\mathbf{x}_K)$ is a.s.). The asymptotic stability is guaranteed regardless of the number of modes in the model or parameter uncertainties. The order of $\boldsymbol{K}$ can be chosen to be any number ≥ 3. In other words, this result enables the design of a controller of any desired order, which robustly stabilizes $\boldsymbol{G}$. A procedure for designing $\boldsymbol{K}$ is to choose $\mathbf{Q}_\mathbf{z} = \mathrm{diag}\,(\mathbf{Q}_K, 0_{3\times 3})$, where $\mathbf{Q}_K = \mathbf{Q}_K^T > 0$, and to choose a stable $\mathbf{A}_K$ and matrices $\mathbf{B}_K$ and $\mathbf{C}_K$ so that equations (A9)

and (A10) are satisfied. Using equation (A8) and defining

$$\mathbf{P_z} = \begin{bmatrix} \mathbf{P_{z1}} & \mathbf{P_{z2}} \\ \mathbf{P_{z2}^T} & \mathbf{P_{z3}} \end{bmatrix}$$

where $\mathbf{P_{z1}}$ is an $n_K \times n_K$ matrix and $\mathbf{P_{z3}}$ is a 3×3 matrix, conditions (ii) and (iii) of theorem 1 can be expanded as:

$$\left.\begin{aligned} &\mathbf{P_{z1}A}_K + \mathbf{A}_K^T\mathbf{P_{z1}} + \mathbf{P_{z2}C}_K + \mathbf{C}_K^T\mathbf{P}_{z2}^T = -\mathbf{L}_K^T\mathbf{L}_K \\ &\mathbf{P}_{z2}^T\mathbf{A}_K + \mathbf{P_{z3}C}_K = 0 \\ &\mathbf{B}_K^T\mathbf{P_{z1}} + \boldsymbol{D}_K^T\mathbf{P}_{z2}^T = 0 \\ &\mathbf{B}_K^T\mathbf{P_{z2}} + \boldsymbol{D}_K^T\mathbf{P_{z3}} = \mathbf{I} \end{aligned}\right\} \quad \text{(A11)}$$

In addition, $\mathbf{P_z}$ must be positive definite. Because of the large number of free parameters (i.e., $\mathbf{A}_K$, $\mathbf{B}_K$, $\mathbf{C}_K$, $\boldsymbol{D}_K$, $\mathbf{L}_K$) it is generally not straightforward to use equation (A11) to obtain the compensator, and this problem remains an area of continuing research. Another method is to use the following s-domain equivalent of theorem 1. (See reference 16.)

Theorem 2

The compensator $\boldsymbol{K}(s)$ stabilizes $\boldsymbol{G}(s)$ if $\boldsymbol{K}(s)$ has no transmission zeros at $s = 0$ and $\boldsymbol{K}(s)/s$ is strongly PR.

The condition that $\boldsymbol{K}(s)/s$ be strongly PR is sometimes much easier to check than the conditions of theorem 1. For example, let $\boldsymbol{K}(s) = \text{diag}\,[K_1(s), K_2(s), K_3(s)]$, where

$$K_i(s) = k_i \frac{s^2 + \beta_{1i}s + \beta_{0i}}{s^2 + \alpha_{1i}s + \alpha_{0i}} \quad \text{(A12)}$$

It is straightforward to show that $\boldsymbol{K}(s)/s$ is strongly PR if (for $i = 1, 2, 3$) $k_i, \alpha_{0i}, \alpha_{1i}, \beta_{0i}$, and β_{1i} are positive, and

$$\alpha_{1i} - \beta_{1i} > 0 \quad \text{(A13)}$$

$$\alpha_{1i}\beta_{0i} - \alpha_{0i}\beta_{1i} > 0 \quad \text{(A14)}$$

For higher order K_i's, the conditions on the polynomial coefficients are harder to obtain. One systematic procedure for obtaining such conditions for higher order controllers is the application of Sturm's theorem (ref. 28). Symbolic manipulation codes can then be used to derive explicit inequalities. The controller design problem can be subsequently posed as a constrained optimization problem that minimizes a given performance function. For the case of fully populated $\boldsymbol{K}(s)$, however, there appear to be no straightforward methods.

The controller $\boldsymbol{K}(s)$ (eqs. (A5) and (A6)) is not strictly proper because of the direct transmission term $\boldsymbol{D}_k$. From a practical viewpoint, it is sometimes desirable to have a strictly proper controller because it attenuates sensor noise as well as high-frequency disturbances. Furthermore, the most common types of controllers, which include the Linear-Quadratic-Gaussian (LQG) as well as the observer-pole placement controllers, are strictly proper (i.e., they have a first-order roll-off). In addition, the realization in equations (A5) and (A6) does not use the rate measurement $\mathbf{y}_r$. The following result from reference 16 states that $\boldsymbol{K}$ can be realized as a strictly proper controller wherein both $\mathbf{y}_p$ and $\mathbf{y}_r$ are used.

Theorem 3

The plant $\boldsymbol{G}(s)$ is stabilized by the controller $\boldsymbol{K}'$ given by

$$\dot{\mathbf{x}}_K = \mathbf{A}_K\mathbf{x}_K + [\mathbf{B}_K - \mathbf{A}_K\mathbf{L}\ \mathbf{L}]\begin{bmatrix}\mathbf{y}_p \\ \mathbf{y}_r\end{bmatrix} \quad \text{(A15)}$$

$$\mathbf{u}_K = \mathbf{C}_K\mathbf{x}_K \quad \text{(A16)}$$

where $\mathbf{L}$ is a solution of

$$\boldsymbol{D}_K - \mathbf{C}_K\mathbf{L} = 0 \quad \text{(A17)}$$

There are many possible solutions for $\mathbf{L}$. The solution that minimizes the Frobenius norm of $\mathbf{L}$ is:

$$\mathbf{L} = \mathbf{C}_K^T\left(\mathbf{C}_K\mathbf{C}_K^T\right)^{-1}\boldsymbol{D}_K \quad \text{(A18)}$$

For the case with no zero-frequency modes, the dynamic dissipative controller degenerates to a positivity controller that uses the feedback of only the velocity. For this case, the robust stability is guaranteed with an SPR dynamic compensator (refs. 30 and 31). In terms of the state equations, it is sufficient for robust stability that the compensator satisfies the Kalman-Yacubovich condition (iii) with $(\boldsymbol{A}, \mathbf{L})$ observable. A simpler sufficient condition, which also involves fewer parameters, is that $\boldsymbol{D}_K = 0$ and $\mathbf{L}$ is a (lower or upper) triangular matrix.

The problem of designing dissipative controllers that also provide optimal performance has been a subject of active research. It has been shown that the static dissipative controller minimizes a certain quadratic performance index (ref. 4). Methods based on eigenstructure assignment with dissipativity constraints have also been recently proposed (ref. 32).

For the case with no zero-frequency modes, it was shown in reference 33 that the selection of LQ regulator and estimator weighting matrices in a certain manner results in an LQG controller that is also SPR, and therefore robustly stabilizes the plant. For the case where zero-frequency modes are present, design methods based on numerical minimization of the "distance" between a nominal LQG controller and dynamic dissipative controllers were suggested in reference 16.

Another approach for the case with zero-frequency modes is a two-level controller wherein an inner loop static dissipative controller with position and velocity feedback is used, and a dynamic dissipative (SPR) velocity feedback controller is used in the outer loop. This approach was discussed in reference 5.

In spite of some progress, the problem of designing *optimal* dissipative controllers remains an area of continuing research.

References

1. Balas, Mark J.: Trends in Large Space Structure Control Theory: Fondest Hopes, Wildest Dreams. *IEEE Trans. Autom. Control*, vol. AC-27, no. 3, June 1982, pp. 522–535.

2. Ketner, G. L.: *Survey of Historical Incidences With Controls-Structures Interaction and Recommended Technology Improvements Needed To Put Hardware in Space.* PNL-6846 (Contract DE-AC06-76R10 1830), Battelle Memorial Inst., Mar. 1989.

3. Newsom, Jerry R.; Layman, W. E.; Waites, H. B.; and Hayduk, R. J.: *The NASA Controls-Structures Interaction Technology Program.* NASA TM-102752, 1990.

4. Joshi, S. M.: *Control of Large Flexible Space Structures.* Volume 131 of *Lecture Notes in Control and Information Sciences,* M. Thoma and A. Wyner, eds., Springer-Verlag, 1989.

5. Joshi, S. M.; and Maghami, P. G.: Dissipative Compensators for Flexible Spacecraft Control. *Proceedings of the 1990 American Control Conference, Volume 2,* IEEE Catalog No. 90CH2896-9, American Automatic Control Council, 1990, pp. 1955–1961.

6. Singiresu, S. Rao; Pan, Tzong-Shii; and Venkayya, Vipperla B.: Robustness Improvement of Actively Controlled Structures Through Structural Modifications. *AIAA J.,* vol. 28, Feb. 1990, pp. 353–361.

7. Balakrishnan, A. V.: Combined Structures-Controls Optimization of Lattice Trusses. *Comput. Methods Appl. Mech. & Eng.,* vol. 94, no. 1, 1992, pp. 131–152.

8. Bossi, J. A.; Hunziker, K. S.; and Kraft, R. H.: *Integrated Control/Structure Design.* NASA CR-182020, 1990.

9. Maghami, P. G.; Walz, J. E.; Joshi, S. M.; and Armstrong, E. S.: Integrated Controls-Structures Design Methodology Development for a Class of Flexible Spacecraft. *Third Air Force/NASA Symposium on Recent Advances in Multidisciplinary Analysis and Optimization—A Collection of Technical Papers,* Sept. 1990, pp. 1–6.

10. Maghami, P. G.; Joshi, S. M.; and Lim, K. B.: Integrated Controls-Structures Design: A Practical Design Tool for Modern Spacecraft. *Proceedings of the 1991 American Control Conference, Volume 2,* IEEE Catalog No. 91CH2939-7, American Automatic Control Council, 1991, pp. 1465–1473.

11. Maghami, P. G.; Joshi, S. M.; Elliot, K. B.; and Walz, J. E.: Integrated Design of the CSI Evolutionary Structure: A Verification of the Design Methodology. Paper presented at the Fifth NASA/DOD Controls-Structures Interaction Conference (Lake Tahoe, Nevada), Mar. 3–5, 1992.

12. Woodard, Stanley E.; Padula, Sharon L.; Graves, Philip C.; and James, Benjamin B.: An Optimization Method for Controlled Space Structures With Variable Actuator Mass. *Proceedings of the Fourth NASA/DOD Controls/Structures Interaction Technology Conference,* Andrew D. Swanson, compiler, WL-TR-91-3013, U.S. Air Force, Jan. 1991, pp. 411–428.

13. Ramler, J.; and Durrett, R.: NASA's Geostationary Communications Platform Program. *A Collection of Technical Papers—AIAA 10th Communication Satellite Systems Conference,* Mar. 1984, pp. 613 621. (Available as AIAA-84-0702.)

14. Belvin, W. Keith; Elliot, Kenny E.; Bruner, Anne; Sulla, Jeff; and Bailey, Jim: The LaRC CSI Phase-0 Evolutionary Model Testbed: Design and Experimental Results. *Proceedings of the Fourth NASA/DOD Controls/Structures Interaction Technology Conference,* Andrew D. Swanson, compiler, WL-TR-91-3013, U.S. Air Force, Jan. 1991, pp. 594–613.

15. Onoda, Junjiro; and Haftka, Raphael T.: Approach to Structure/Control Simultaneous Optimization of Large Flexible Spacecraft. *AIAA J.,* vol. 25, no. 8, Aug. 1987, pp. 1133–1138.

16. Joshi, S. M.; Maghami, P. G.; and Kelkar, A. G.: Dynamic Dissipative Compensator Design for Large Space Structures. *A Collection of Technical Papers, Volume 1—AIAA Guidance, Navigation and Control Conference,* Aug. 1991, pp. 467–477. (Available as AIAA-91-2650-CP.)

17. Lefschetz, Solomon: *Stability of Nonlinear Control Systems.* Academic Press Inc., 1965.

18. Jamshidi, M.; and Herget, C. J., eds.: *Computer-Aided Control Systems Engineering.* North Holland, c.1985.

19. Fenves, Steven J.; Perrone, Nicholas; Robinson, Arthur R.; and Schnobrich, William C., eds.: *Numerical and Computer Methods in Structural Mechanics.* Academic Press, Inc., 1973.

20. Belvin, W. Keith; and Park, K. C.: Computer Implementation of Analysis and Optimization Procedures for Control-Structure Interaction Problems. *A Collection of Technical Papers—AIAA Dynamics Specialist Conference,* Apr. 1990, pp. 32–41. (Available as AIAA-90-1194-CP.)

21. Vanderplaats, G. N.: *ADS—A Fortran Program for Automated Design Synthesis—Version 1.10.* NASA CR-177985, 1985.

22. Vanderplaats, Garret N.: *Numerical Optimization Techniques for Engineering Design—With Applications.* McGraw-Hill, Inc., c.1984.

23. George, Alan; and Liu, Joseph W.-H.: *Computer Solution of Large Sparse Positive Definite Systems.* Prentice-Hall, Inc., c.1981.

24. Kenny, Sean P.; Hou, Gene J.; and Belvin, W. Keith: Eigensensitivity in Integrated Design. *Proceedings of the Fourth NASA/DOD Controls/Structures Interaction Technology Conference,* Andrew D. Swanson, compiler, WL-TR-91-3013, U.S. Air Force, Jan. 1991, pp. 31–40.

25. Stengel, Robert F.: *Stochastic Optimal Control—Theory and Application.* John Wiley & Sons, Inc., c.1986.

26. Popov, V. M.: *Hyperstability of Control Systems.* Springer-Verlag, 1973.

27. Anderson, B. D. O.: A System Theory Criterion for Positive Real Matrices. *SIAM J. Control,* vol. 5, no. 2, May 1967, pp. 171–182.

28. Van Valkenberg, M. E.: *Introduction to Modern Network Synthesis.* John Wiley & Sons, Inc., c.1960.

29. Lozano-Leal, Rogelio; and Joshi, Suresh M.: Strictly Positive Real Functions Revisited. *IEEE Trans. Autom. Control,* vol. 35, no. 11, Nov. 1990, pp. 1243–1245.

30. Benhabib, R. J.; Iwens, R. P.; and Jackson, R. L.: Stability of Large Space Structure Control Systems Using Positivity Concepts. *J. Guid. & Control,* vol. 4, no. 5, Sept.–Oct. 1981, pp. 487–494.

31. McLaren, M. D.; and Slater, G. L.: Robust Multivariable Control of Large Space Structures Using Positivity. *J. Guid., Control, & Dyn.,* vol. 10, no. 4, July–Aug. 1987, pp. 393–400.

32. Maghami, P. G.; Gupta, S.; and Joshi, S. M.: Design of Dissipative Low-Authority Controllers Using an Eigensystem Assignment Technique. Paper presented at 1992 American Control Conference (Chicago, Illinois), June 24–26, 1992.

33. Lozano-Leal, R.; and Joshi, S. M.: On the Design of Dissipative LQG-Type Controllers. *Recent Advances in Robust Control,* Peter Dorato and Rama K. Yedavalli, eds., Inst. of Electrical and Electronics Engineers, Inc., c.1990, pp. 251–252.

Table 1. Open-Loop Modal Frequencies for the Nominal EPS Model

Mode	Frequency, Hz
1	0.58
2	0.73
3	0.91
4	2.40
5	2.99
6	3.18
7	6.65
8	7.36
9	16.31
10	17.73

Table 2. Integrated Design of the EPS Model for Design Problem I

[Static dissipative controller]

Design	RMS pointing, μrad	Structural mass, kg	Actuator mass, kg	Control power, $N^2 \cdot m^2$
Initial design	73.6	442.06	150	2.98
Control-optimized design	26.78	442.06	150	3.00
Integrated design (without actuator mass)	16.78	437.34	150	3.00
Integrated design (with actuator mass)	17.01	400.32	298.73	3.00

Table 3. Optimization Data and Results for the Structural Design Variables of the EPS Model for Design Problem I

Design variables	Section	Upper bound values, m	Lower bound values, m	Initial values, m	Final values, m
1 (longeron)	1	0.15	0.01	0.051	0.107
2 (batten)	1	.15	.01	.051	.030
3 (diagonal)	1	.15	.01	.051	.025
4 (longeron)	2	0.15	0.01	0.051	0.066
5 (batten)	2	.15	.01	.051	.010
6 (diagonal)	2	.15	.01	.051	.010
7 (longeron)	3	0.15	0.01	0.051	0.066
8 (batten)	3	.15	.01	.051	.041
9 (diagonal)	3	.15	.01	.051	.058
10 (support)	Large antenna	0.15	0.01	0.051	0.149
11 (support)	Small antenna	0.15	0.01	0.051	0.010

Table 4. Modal Frequencies for the Redesigned EPS Model for Design Problem I

Mode	Frequency, Hz
1	0.17
2	.22
3	.23
4	2.75
5	3.11
6	3.30
7	5.98
8	6.62
9	8.58
10	14.13

Table 5. Elements of Cholesky Matrices for the Attitude and Rate Gain Matrices of the EPS Model for Design Problem I

Design variable	Nominal design	Control-optimized design	Integrated design
$\mathbf{L}_p(1,1)$	120.0	188.7	254.3
$\mathbf{L}_p(2,1)$	0	7.1	1.2
$\mathbf{L}_p(3,1)$	0	3.9	−1.7
$\mathbf{L}_p(2,2)$	180.0	179.2	245.0
$\mathbf{L}_p(3,2)$	0	7.4	0.6
$\mathbf{L}_p(3,3)$	240.0	189.9	255.7
$\mathbf{L}_r(1,1)$	90.0	212.5	223.2
$\mathbf{L}_r(2,1)$	0	−17.4	−2.9
$\mathbf{L}_r(3,1)$	0	15.3	8.3
$\mathbf{L}_r(2,2)$	150.0	272.1	327.9
$\mathbf{L}_r(3,2)$	0	−33.0	−1.0
$\mathbf{L}_r(3,3)$	200.0	293.8	403.3

Table 6. Integrated Design of the EPS Model for Design Problem II (Static Dissipative Controller)

[rms < 11 μrad]

Design	Normalized controlled performance	Normalized structural mass	Normalized actuator mass	Normalized total mass
Initial design	1.0	1.0	1.0	1.0
Control-optimized design, $\beta = 0.50$	1.44	1.0	1.33	1.01
Integrated design, $\beta = 0.50$	2.34	.47	.76	.95

Table 7. Optimization Data and Results for the Structural Design Variables of the EPS Model for Design Problem II

Design variable	Section	Upper bound values, m	Lower bound values, m	Initial values, m	Final values, m
1 (longeron)	1	0.15	0.01	0.051	0.010
2 (batten)	1	.15	.01	.051	.010
3 (diagonal)	1	.15	.01	.051	.010
4 (longeron)	2	0.15	0.01	0.051	0.018
5 (batten)	2	.15	.01	.051	.010
6 (diagonal)	2	.15	.01	.051	.010
7 (longeron)	3	0.15	0.01	0.051	0.010
8 (batten)	3	.15	.01	.051	.010
9 (diagonal)	3	.15	.01	.051	.010
10 (support)	Large antenna	0.15	0.01	0.051	0.114
11 (support)	Small antenna	0.15	0.01	0.051	0.083

Table 8. Modal Frequencies for the Redesigned EPS Model for Design Problem II

Mode	Frequency, Hz
1	1.79
2	2.04
3	2.16
4	3.48
5	3.76
6	4.63
7	5.52
8	5.74
9	9.26
10	9.71

Table 9. Elements of Cholesky Matrices for the Attitude and Rate Gain Matrices of the EPS Model for Design Problem II

Design variable	Nominal design	Control-optimized design	Integrated design
$\mathbf{L}_p(1,1)$	120.0	201.9	178.4
$\mathbf{L}_p(2,1)$	0	1.2	−.005
$\mathbf{L}_p(3,1)$	0	1.5	−.001
$\mathbf{L}_p(2,2)$	180.0	254.3	178.4
$\mathbf{L}_p(3,2)$	0	1.8	.012
$\mathbf{L}_p(3,3)$	240.0	254.6	178.3
$\mathbf{L}_r(1,1)$	90.0	184.0	206.0
$\mathbf{L}_r(2,1)$	0	4.3	.001
$\mathbf{L}_r(3,1)$	0	−1.8	.002
$\mathbf{L}_r(2,2)$	150.0	251.5	205.5
$\mathbf{L}_r(3,2)$	0	−2.4	−.006
$\mathbf{L}_r(3,3)$	200.0	252.0	200.9

Table 10. Modal Frequencies for the CSI Phase-0 Evolutionary Model

Mode	Frequency, Hz
1	0.122
2	.126
3	.173
4	.680
5	.704
6	1.159
7	1.572
8	1.676
9	2.085
10	3.867
11	3.972
12	4.127
13	4.172
14	5.788
15	6.456
16	6.568
17	6.777
18	7.806
19	8.732
20	9.396

Table 11. Integrated Design of the CSI Evolutionary Model

[Static dissipative controller]

Design	rms displacement, in.	Control power, lb^2	Transient controlled performance, P_c
Control-optimized design	1.70	19.34	0.0048
Integrated design	1.70	11.41	.0038

Table 12. Optimization Data and Results for the Structural Design Variables of the CSI Evolutionary Model

[Static dissipative controller]

Design variable	Section	Upper bound values, in.	Lower bound values, in.	Initial values, in.	Final values, in.
1 (longeron)	1	1.0	0.12	0.3125	0.999
2 (batten)	1	1.0	.12	.3125	.633
3 (diagonal)	1	1.0	.12	.3125	.958
4 (longeron)	2	1.0	0.12	0.3125	0.124
5 (batten)	2	1.0	.12	.3125	.644
6 (diagonal)	2	1.0	.12	.3125	.144
7 (longeron)	3	1.0	0.12	0.3125	0.999
8 (batten)	3	1.0	.12	.3125	.453
9 (diagonal)	3	1.0	.12	.3125	.658
10 (longeron)	4	1.0	0.12	0.3125	1.000
11 (batten)	4	1.0	.12	.3125	.181
12 (diagonal)	4	1.0	.12	.3125	.407
13 (longeron)	5	1.0	0.12	0.3125	0.425
14 (batten)	5	1.0	.12	.3125	.143
15 (diagonal)	5	1.0	.12	.3125	.138
16 (longeron)	6	1.0	0.12	0.3125	0.122
17 (batten)	6	1.0	.12	.3125	.392
18 (diagonal)	6	1.0	.12	.3125	.145
19 (longeron)	7	1.0	0.12	0.3125	0.142
20 (batten)	7	1.0	.12	.3125	.183
21 (diagonal)	7	1.0	.12	.3125	.427

Table 13. Modal Frequencies for the Redesigned CSI Evolutionary Model

[Static dissipative controller]

Mode	Frequency, Hz
1	0.122
2	.127
3	.173
4	.625
5	.684
6	1.191
7	1.642
8	2.334
9	2.651
10	3.829
11	3.995
12	4.226
13	4.598
14	5.379
15	7.092
16	7.639
17	7.910
18	8.599
19	8.994
20	9.020

Table 14. Diagonal Elements of Rate Gain Matrix for the CSI Evolutionary Model

[Static dissipative controller]

Design variable	Control-optimized design	Integrated design
$\mathbf{G}_r(1,1)$	1.525	1.263
$\mathbf{G}_r(2,2)$	.409	.477
$\mathbf{G}_r(3,3)$	1.234	1.203
$\mathbf{G}_r(4,4)$	.448	.440
$\mathbf{G}_r(5,5)$	2.126	1.674
$\mathbf{G}_r(6,6)$	2.122	1.671
$\mathbf{G}_r(7,7)$	.352	.869
$\mathbf{G}_r(8,8)$	.680	.626

Table 15. Integrated Design of the CSI Evolutionary Model

[Dynamic dissipative controller]

Design	RMS displacement, in.	Control power, lb^2	Transient controlled performance, P_c
Control-optimized design	1.70	8.31	0.0026
Integrated design	1.70	5.91	.0024

Table 16. Optimization Data and Results for Structural Design Variables of the CSI Evolutionary Model

[Dynamic dissipative controller]

Design variable	Section	Upper bound values, in.	Lower bound values, in.	Initial values, in.	Final values, in.
1 (longeron)	1	1.0	0.12	0.3125	0.999
2 (batten)	1	1.0	.12	.3125	.547
3 (diagonal)	1	1.0	.12	.3125	1.000
4 (longeron)	2	1.0	0.12	0.3125	0.120
5 (batten)	2	1.0	.12	.3125	.540
6 (diagonal)	2	1.0	.12	.3125	.120
7 (longeron)	3	1.0	0.12	0.3125	1.000
8 (batten)	3	1.0	.12	.3125	.354
9 (diagonal)	3	1.0	.12	.3125	.579
10 (longeron)	4	1.0	0.12	0.3125	1.000
11 (batten)	4	1.0	.12	.3125	.138
12 (diagonal)	4	1.0	.12	.3125	.367
13 (longeron)	5	1.0	0.12	0.3125	0.357
14 (batten)	5	1.0	.12	.3125	.120
15 (diagonal)	5	1.0	.12	.3125	.120
16 (longeron)	6	1.0	0.12	0.3125	0.120
17 (batten)	6	1.0	.12	.3125	.308
18 (diagonal)	6	1.0	.12	.3125	.120
19 (longeron)	7	1.0	0.12	0.3125	0.120
20 (batten)	7	1.0	.12	.3125	.135
21 (diagonal)	7	1.0	.12	.3125	.332

Table 17. Modal Frequencies for the Redesigned CSI Evolutionary Model

[Dynamic dissipative controller]

Mode	Frequency, Hz
1	0.122
2	.127
3	.173
4	.629
5	.690
6	1.186
7	1.578
8	2.238
9	2.576
10	3.761
11	3.782
12	4.174
13	4.320
14	5.196
15	6.443
16	7.351
17	7.876
18	8.549
19	8.922
20	8.982

Table 18. Control Design Variables for the CSI Evolutionary Model

[Dynamic dissipative controller]

Design variable	Control-optimized design	Integrated design
$\mathbf{A}_c(2,1)$	11.400	45.204
$\mathbf{A}_c(2,2)$	66.351	107.918
$\mathbf{A}_c(4,3)$	82.667	72.342
$\mathbf{A}_c(4,4)$	92.846	80.691
$\mathbf{A}_c(6,5)$	20.989	35.454
$\mathbf{A}_c(6,6)$	70.983	94.716
$\mathbf{A}_c(8,7)$	89.514	74.961
$\mathbf{A}_c(8,8)$	92.700	79.441
$\mathbf{A}_c(10,9)$	27.749	43.161
$\mathbf{A}_c(10,10)$	42.645	88.555
$\mathbf{A}_c(12,11)$	21.109	44.916
$\mathbf{A}_c(12,12)$	50.887	91.610
$\mathbf{A}_c(14,13)$	21.495	38.261
$\mathbf{A}_c(14,14)$	100.329	86.221
$\mathbf{A}_c(16,15)$	22.814	29.081
$\mathbf{A}_c(16,16)$	81.224	90.669

Table 19. Control Design Variables for the CSI Evolutionary Model

[Dynamic dissipative controller]

Design variable	Control-optimized design	Integrated design
$\mathbf{Q}(1,1)$	1903.7	13 117.1
$\mathbf{Q}(2,2)$	3585.4	10 156.0
$\mathbf{Q}(3,3)$	3126.9	2 632.3
$\mathbf{Q}(4,4)$	3155.5	2 472.4
$\mathbf{Q}(5,5)$	3704.8	8 693.4
$\mathbf{Q}(6,6)$	3054.8	5 610.7
$\mathbf{Q}(7,7)$	3008.7	2 292.9
$\mathbf{Q}(8,8)$	3047.9	2 254.9
$\mathbf{Q}(9,9)$	4088.5	12 123.5
$\mathbf{Q}(10,10)$	2279.1	8 354.5
$\mathbf{Q}(11,11)$	3018.3	11 099.9
$\mathbf{Q}(12,12)$	3302.3	9 466.5
$\mathbf{Q}(13,13)$	4205.1	6 252.3
$\mathbf{Q}(14,14)$	2455.0	3 939.0
$\mathbf{Q}(15,15)$	3711.6	4 858.3
$\mathbf{Q}(16,16)$	2917.6	3 167.5

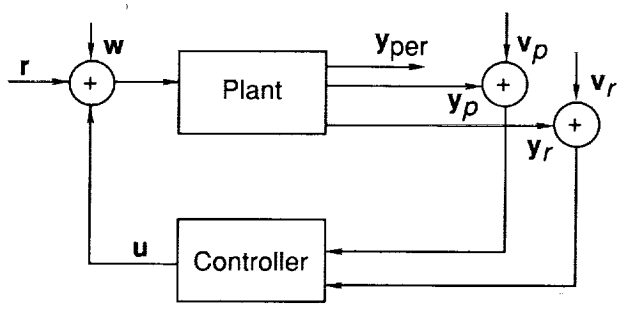

Figure 1. Block diagram for a general system configuration.

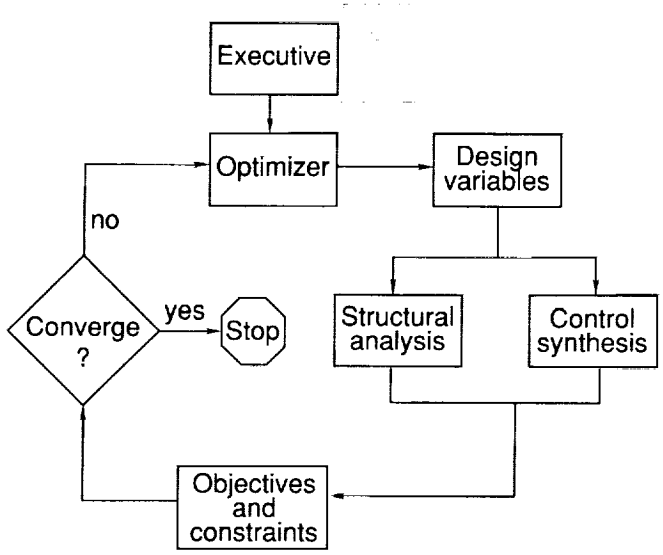

Figure 2. Flow diagram for the integrated controls-structures optimization.

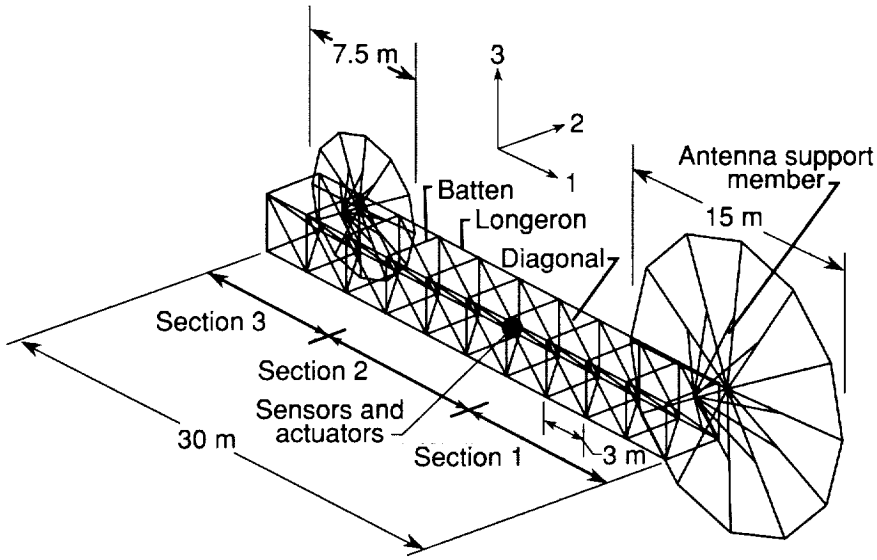

Figure 3. Schematic of the EPS.

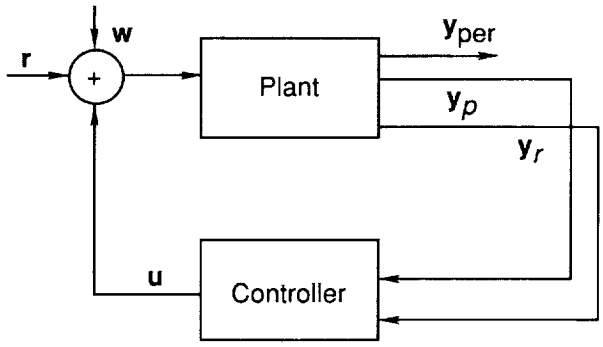

Figure 4. Block diagram of the system configuration for design problem I.

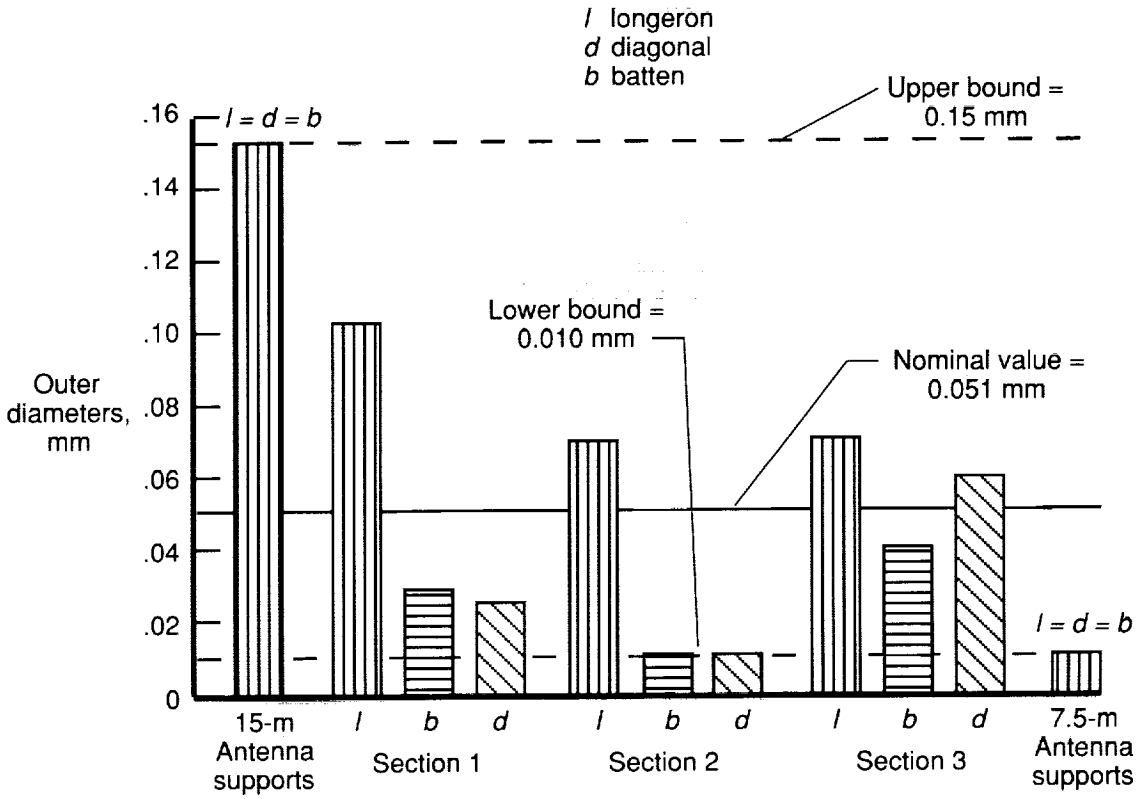

Figure 5. Optimized structural parameters for the EPS Model for design problem I.

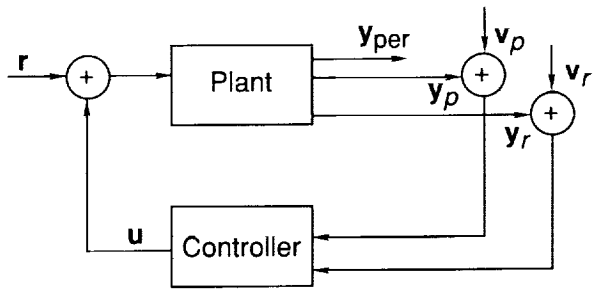

Figure 6. Block diagram of the system configuration for design problem II.

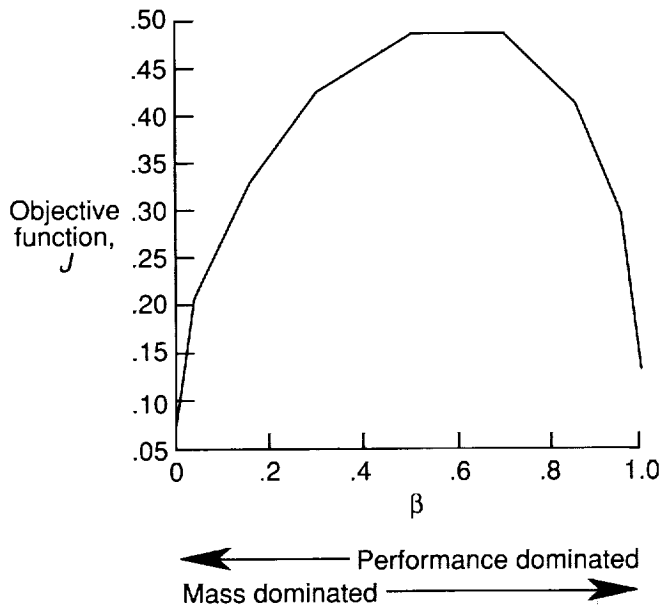

(a) Objective function versus β.

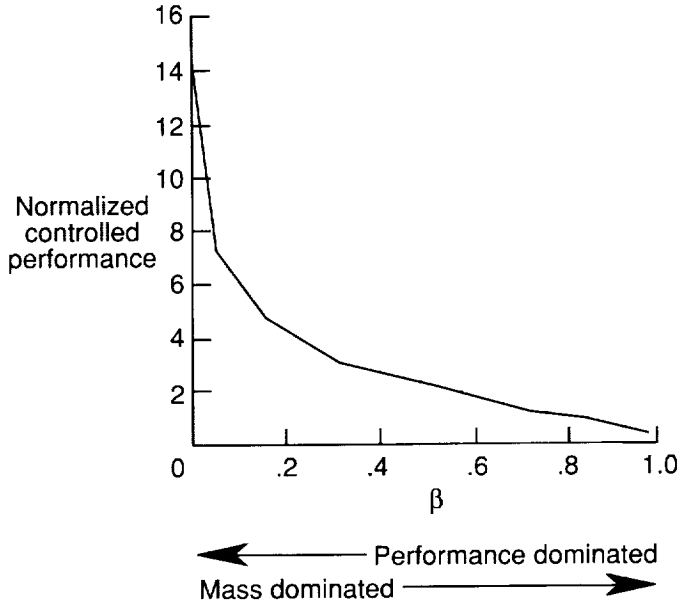

(b) Normalized controlled performance versus β.

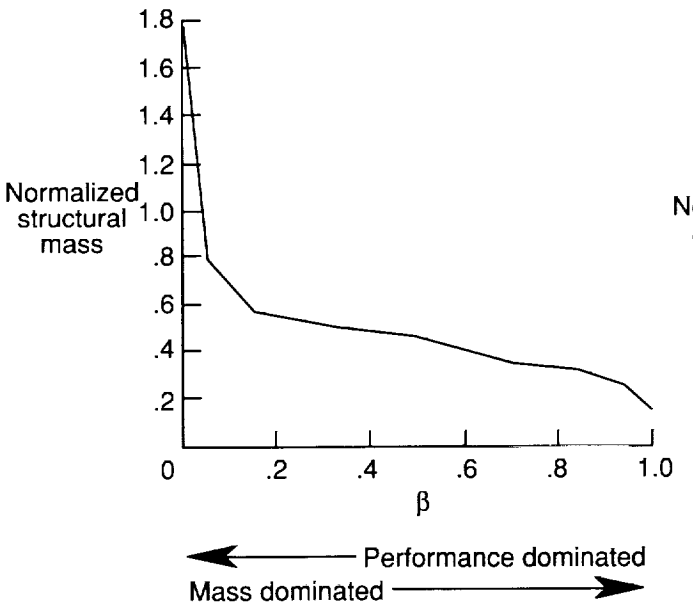

(c) Normalized structural mass versus β.

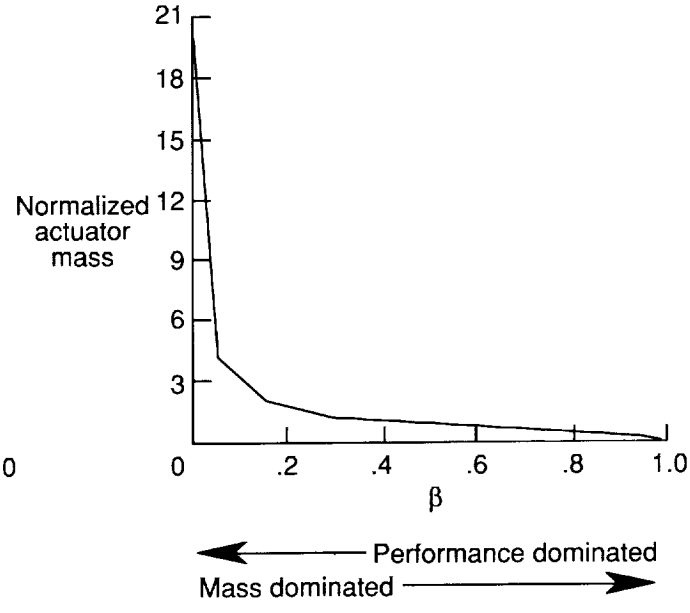

(d) Normalized actuator mass versus β.

Figure 7. Controls-structures trade-off study for the EPS Model.

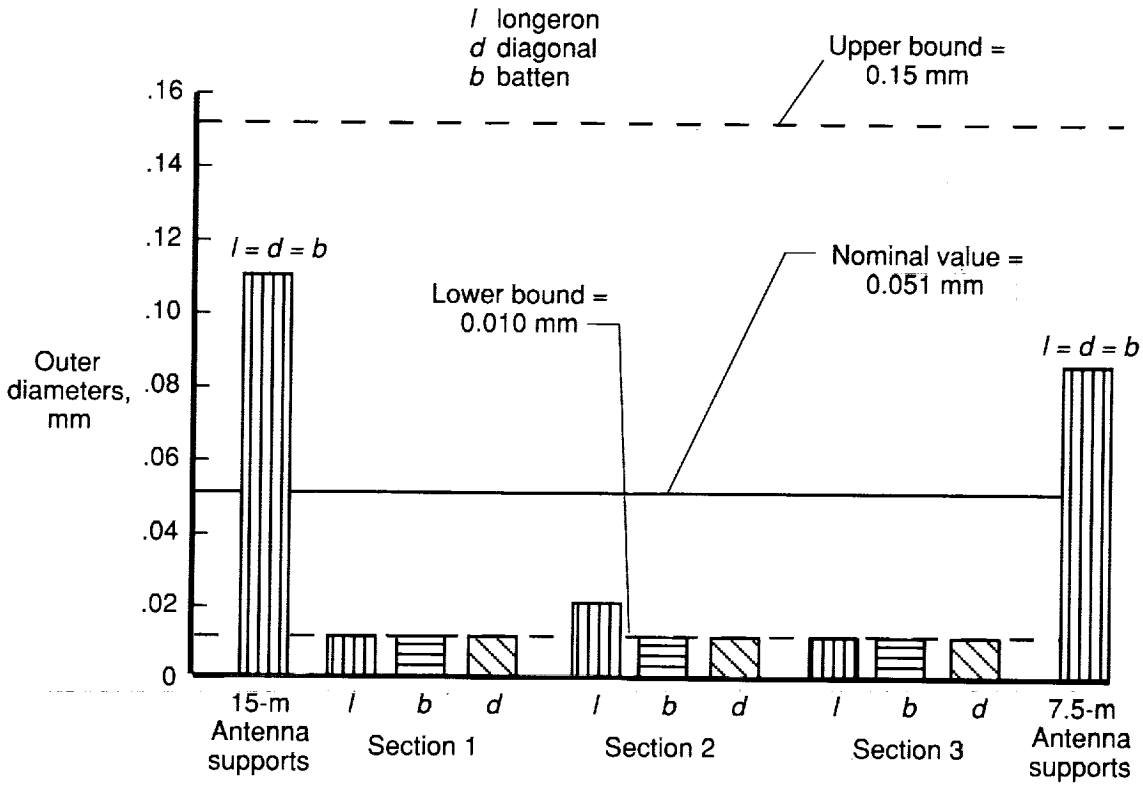

Figure 8. Optimized structural parameters of the EPS Model for design problem II.

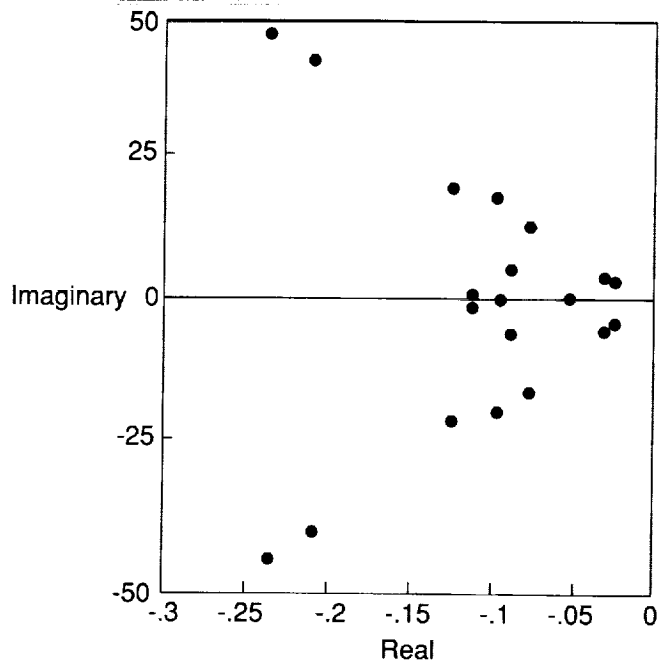

Figure 9. Closed-loop eigenvalues of the EPS model for design problem II—nominal controller design.

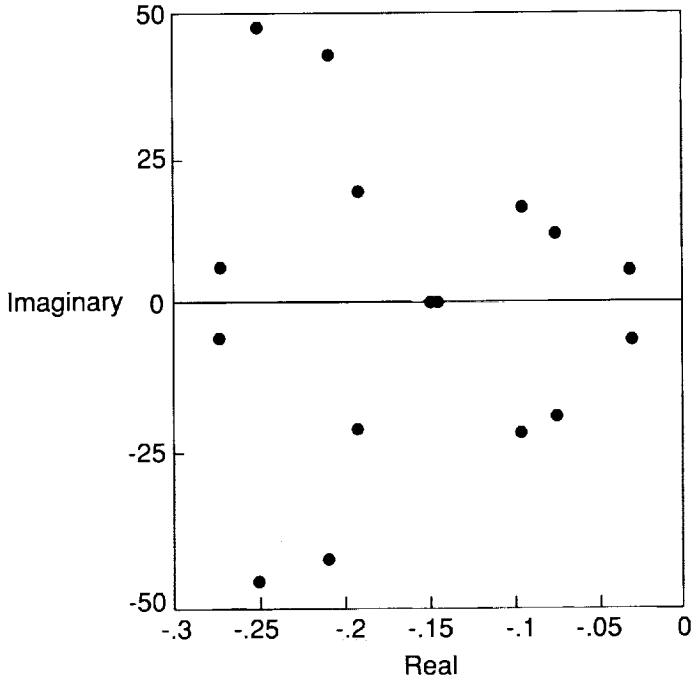

Figure 10. Closed-loop eigenvalues of the EPS model for design problem II—control-optimized design.

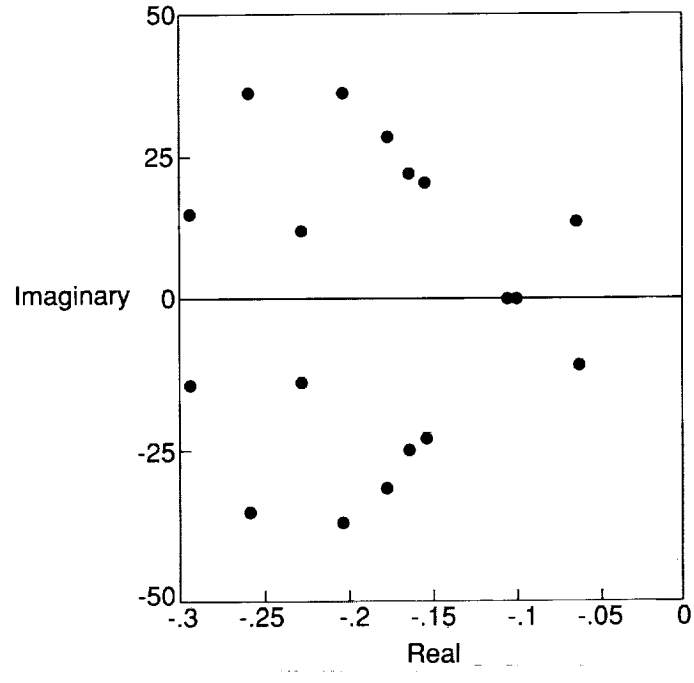

Figure 11. Closed-loop eigenvalues of the EPS model for design problem II—integrated controls-structures design.

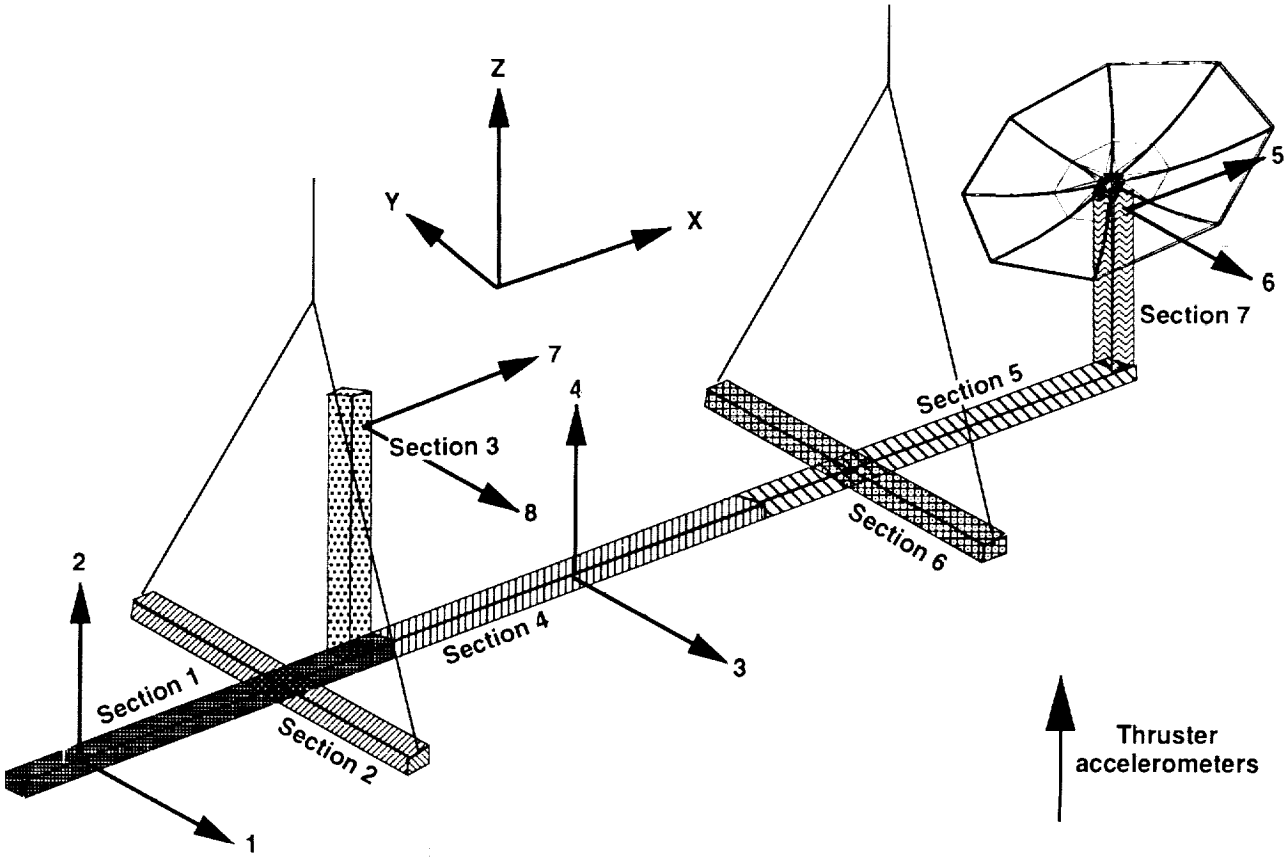

Figure 12. Schematic of the CSI Phase-0 Evolutionary Model.

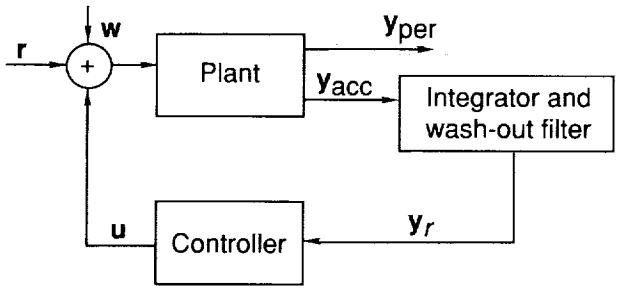

Figure 13. Block diagram of the system configuration for the CSI Evolutionary Model.

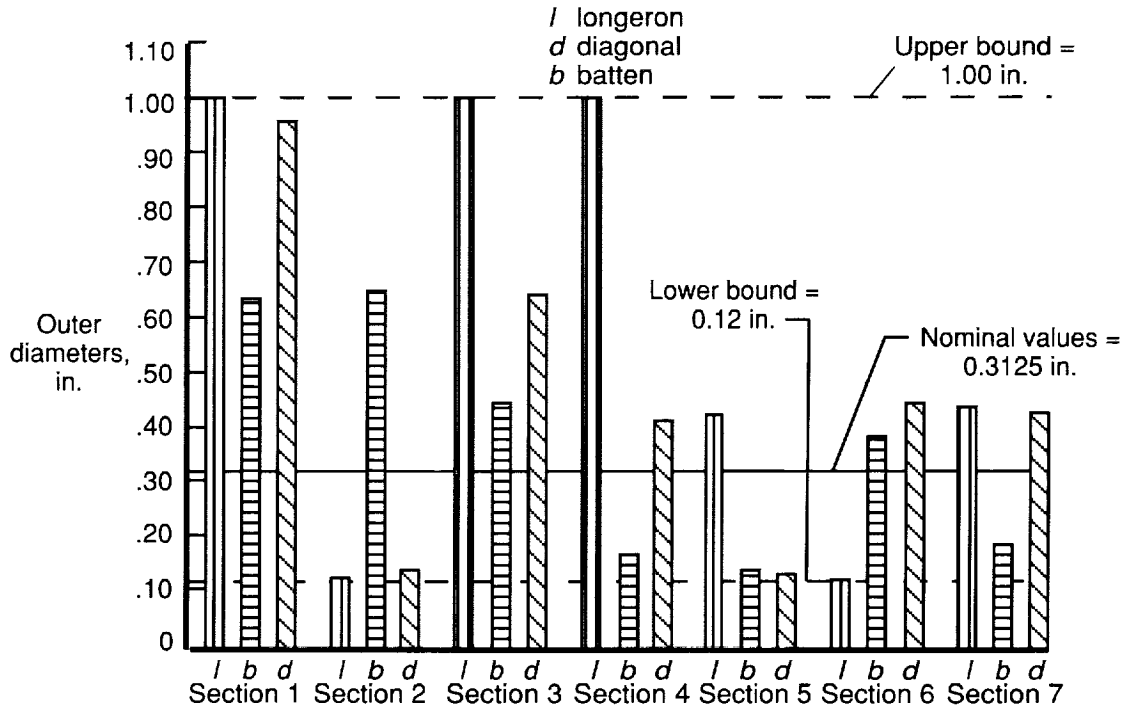

Figure 14. Optimized structural parameters for the CSI Evolutionary Model—static dissipative controller.

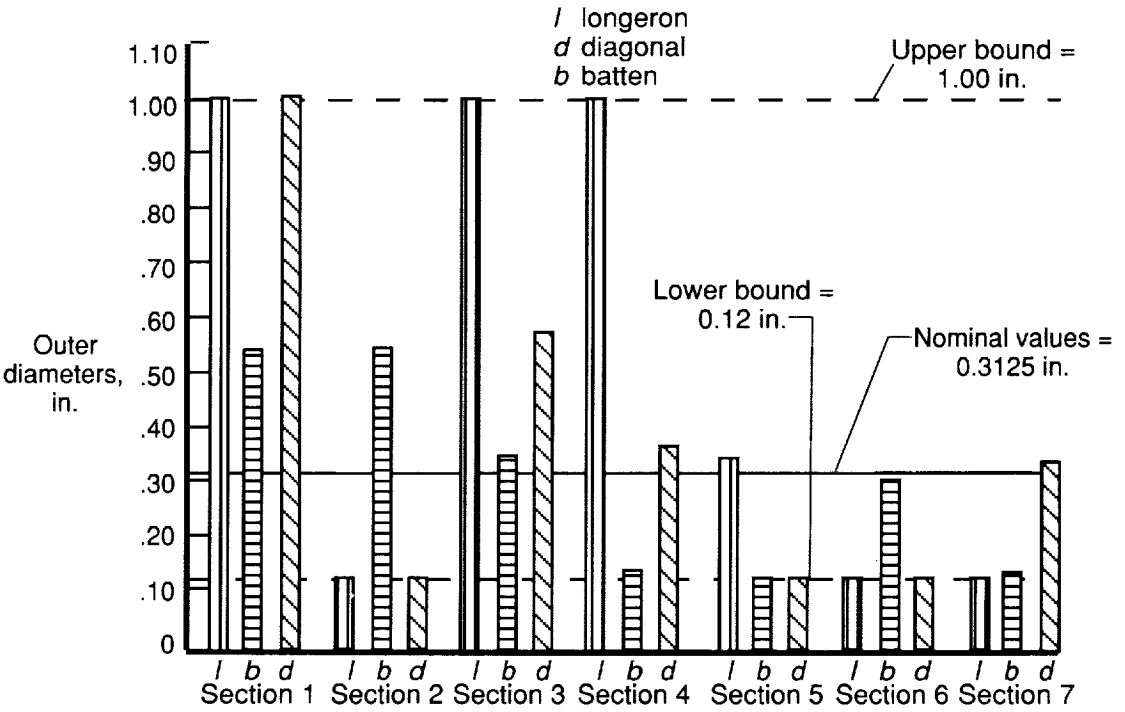

Figure 15. Optimized structural parameters for the CSI Evolutionary Model—dynamic dissipative controller.

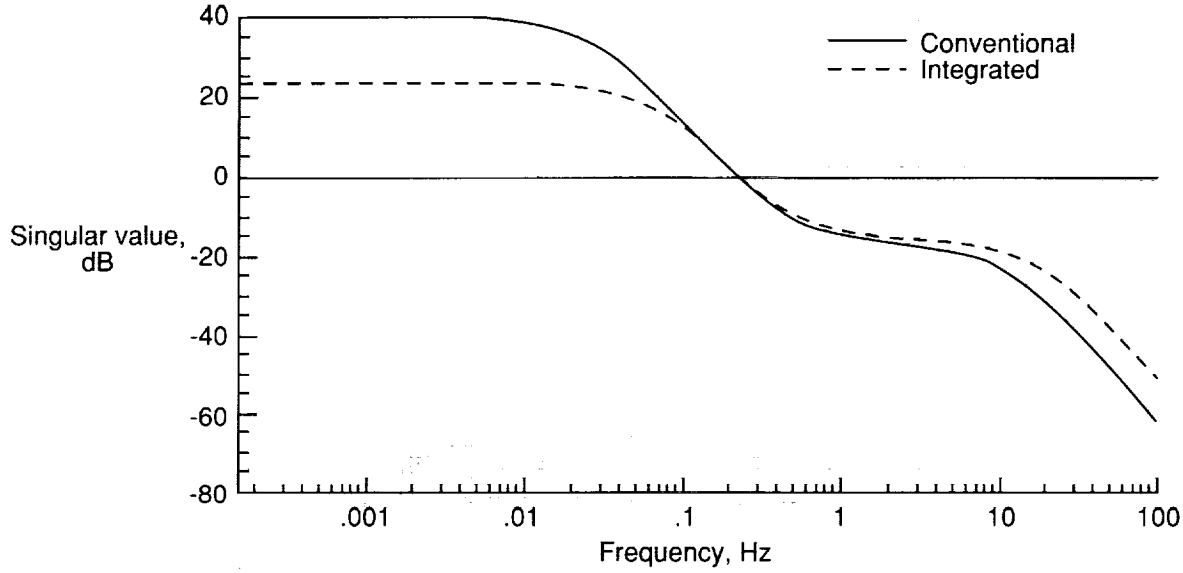

(a) Input/output channel 1.

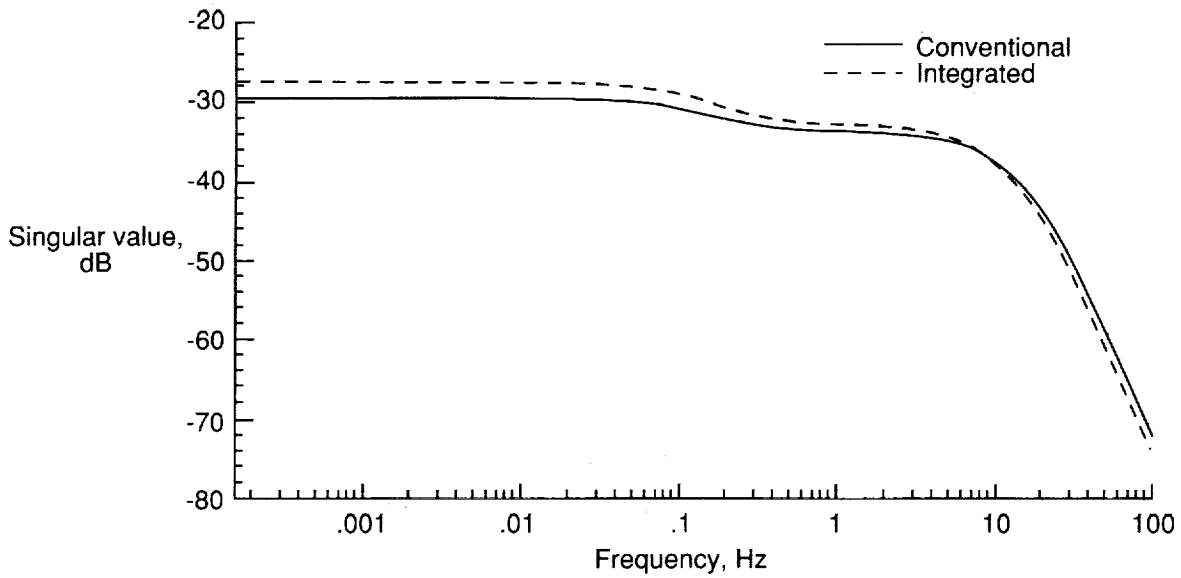

(b) Input/output channel 2.

Figure 16. Singular value plots for input/output channels of the dynamic dissipative controller—the CSI Evolutionary Model.

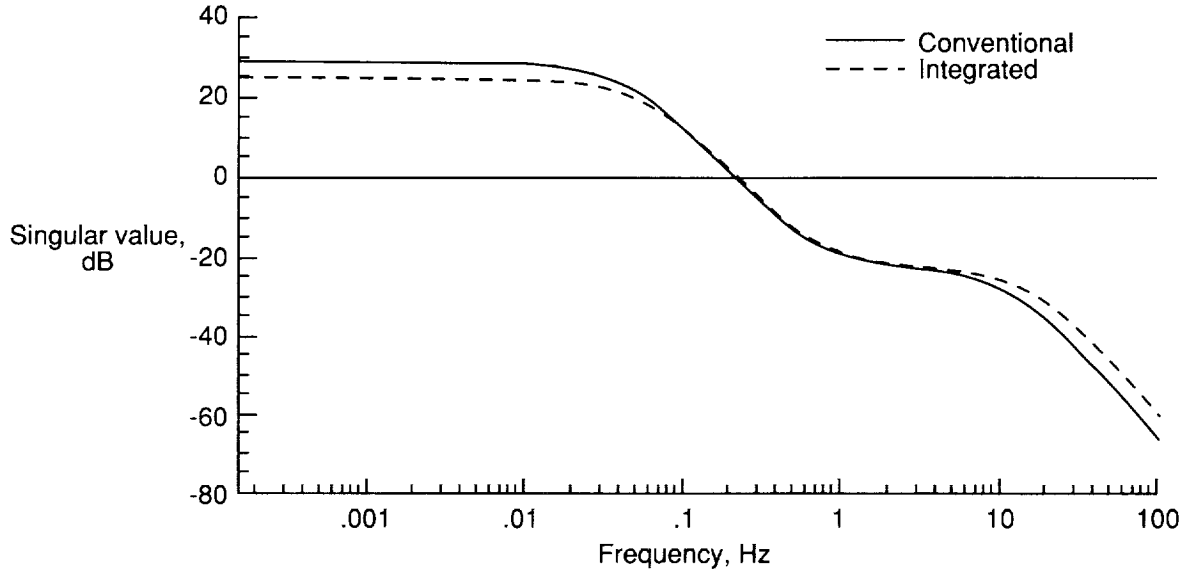

(c) Input/output channel 3.

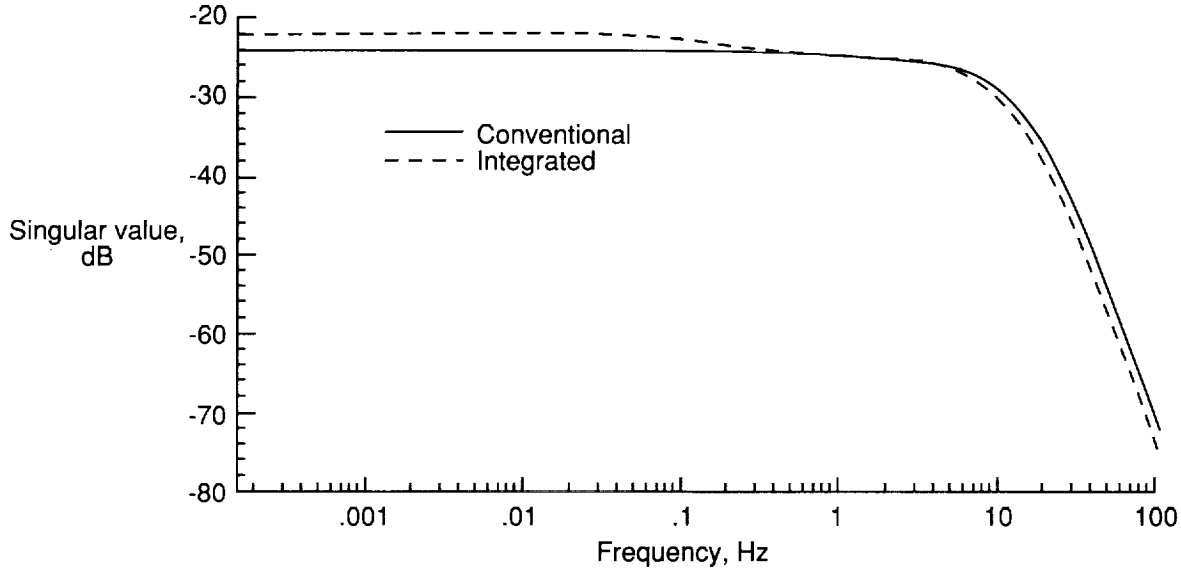

(d) Input/output channel 4.

Figure 16. Continued.

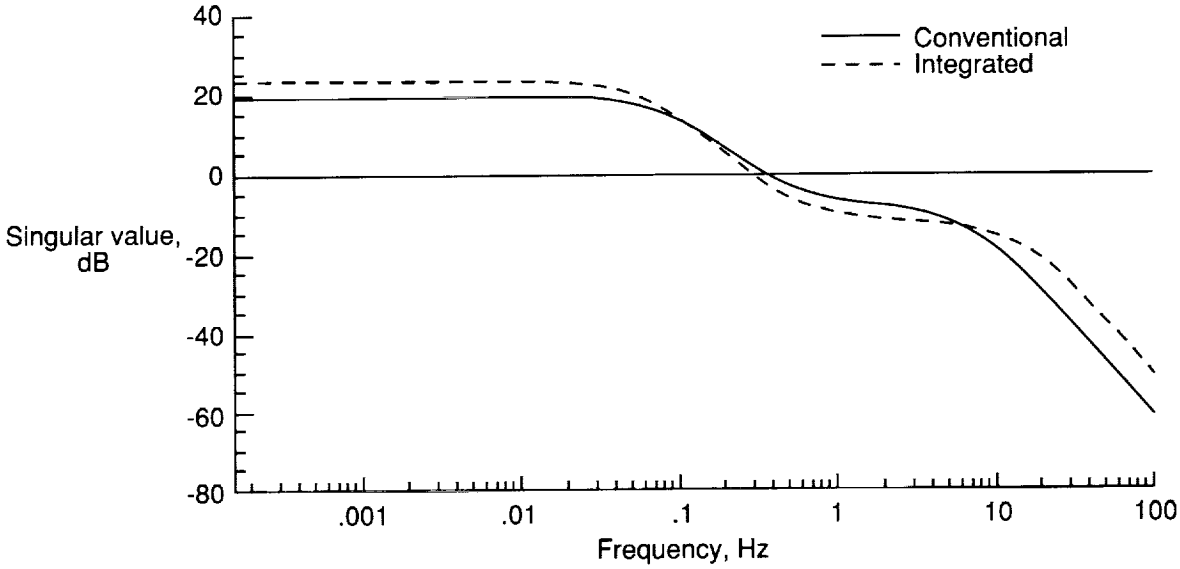

(e) Input/output channel 5.

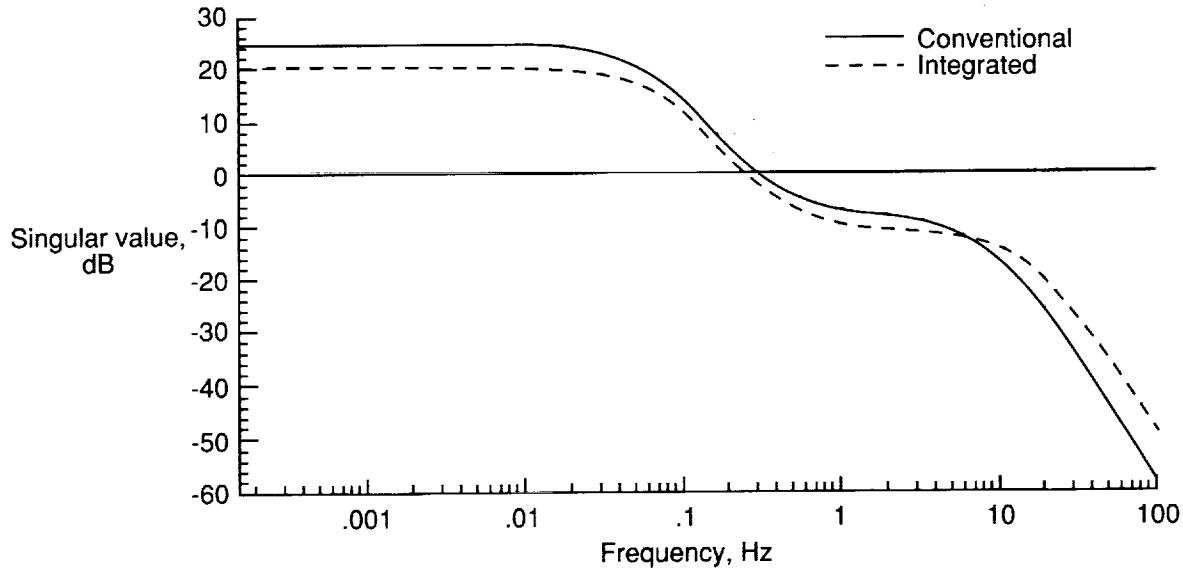

(f) Input/output channel 6.

Figure 16. Continued.

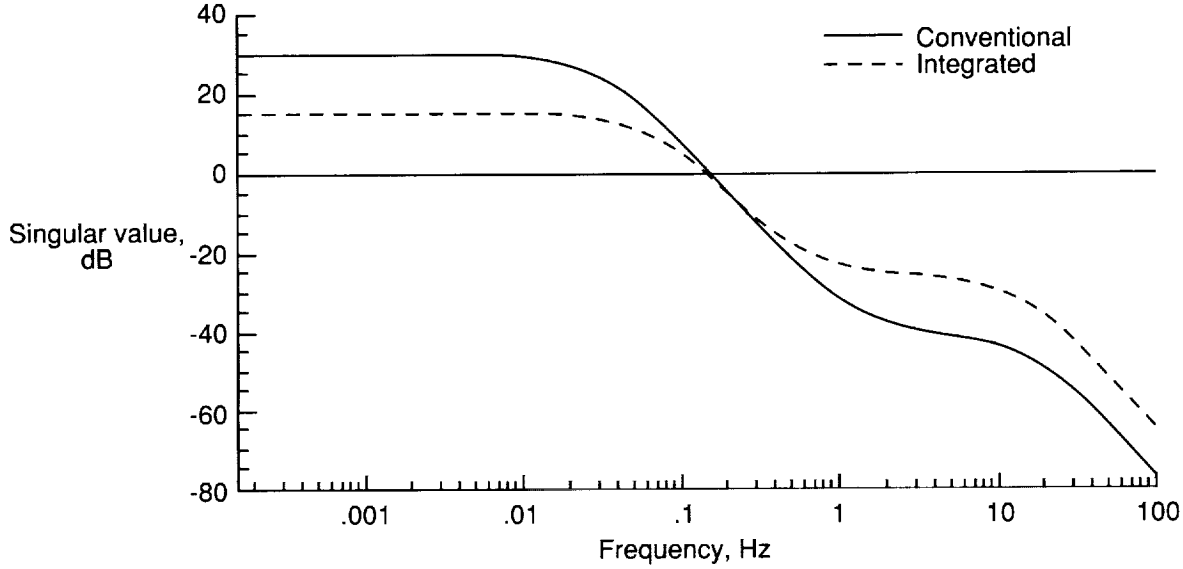

(g) Input/output channel 7.

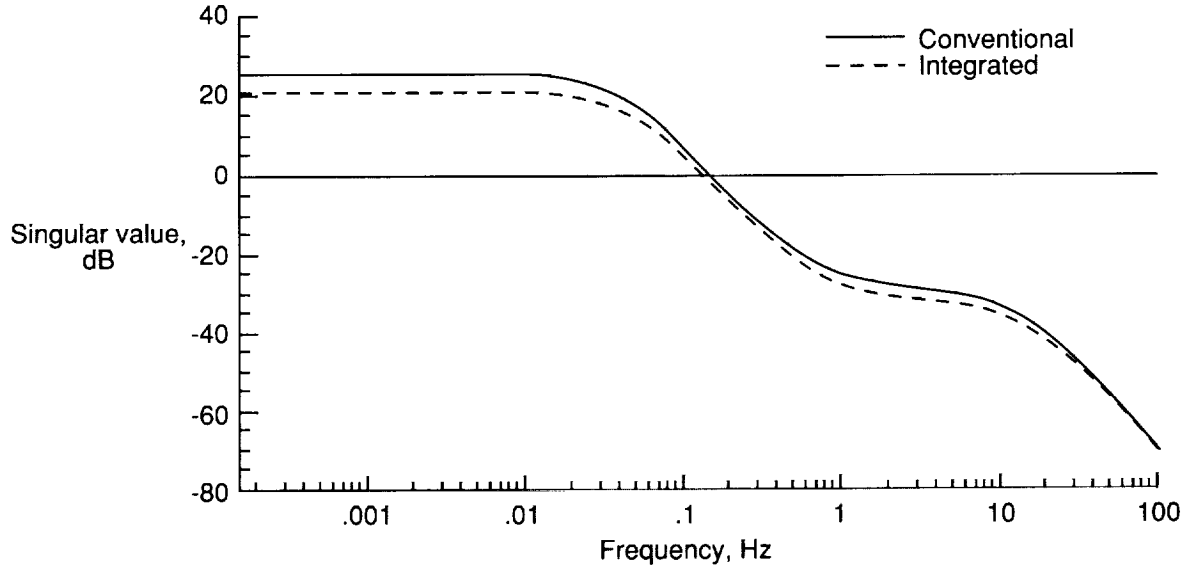

(h) Input/output channel 8.

Figure 16. Concluded.

REPORT DOCUMENTATION PAGE

Form Approved
OMB No. 0704-0188

1. AGENCY USE ONLY *(Leave blank)*	2. REPORT DATE	3. REPORT TYPE AND DATES COVERED
	January 1993	Technical Paper

4. TITLE AND SUBTITLE
An Optimization-Based Integrated Controls-Structures Design Methodology for Flexible Space Structures

5. FUNDING NUMBERS
WU 590-14-51-01

6. AUTHOR(S)
Peiman G. Maghami, Suresh M. Joshi, and Ernest S. Armstrong

7. PERFORMING ORGANIZATION NAME(S) AND ADDRESS(ES)
NASA Langley Research Center
Hampton, VA 23681-0001

8. PERFORMING ORGANIZATION REPORT NUMBER
L-17080

9. SPONSORING/MONITORING AGENCY NAME(S) AND ADDRESS(ES)
National Aeronautics and Space Administration
Washington, DC 20546-0001

10. SPONSORING/MONITORING AGENCY REPORT NUMBER
NASA TP-3283

11. SUPPLEMENTARY NOTES

12a. DISTRIBUTION/AVAILABILITY STATEMENT
Unclassified–Unlimited

Subject Category 18

12b. DISTRIBUTION CODE

13. ABSTRACT *(Maximum 200 words)*

An approach for an optimization-based integrated controls-structures design is presented for a class of flexible spacecraft that require fine attitude pointing and vibration suppression. The integrated design problem is posed in the form of simultaneous optimization of both structural and control design variables. The approach is demonstrated by application to the integrated design of a generic space platform and to a model of a ground-based flexible structure. The numerical results obtained indicate that the integrated design approach can yield spacecraft designs that have substantially superior performance over a conventional design wherein the structural and control designs are performed sequentially. For example, a 40-percent reduction in the pointing error is observed along with a slight reduction in mass, or an almost twofold increase in the controlled performance is indicated with more than a 5-percent reduction in the overall mass of the spacecraft (a reduction of hundreds of kilograms).

14. SUBJECT TERMS
Structures; Controls; Conventional design; Integrated design; Optimization

15. NUMBER OF PAGES
44

16. PRICE CODE
A03

17. SECURITY CLASSIFICATION OF REPORT	18. SECURITY CLASSIFICATION OF THIS PAGE	19. SECURITY CLASSIFICATION OF ABSTRACT	20. LIMITATION OF ABSTRACT
Unclassified	Unclassified		